

A review on the effect of laser pulse shaping on the microstructure and hot cracking behavior in the welding of alloys

Peilei Zhang^{a,b,c*}, Zhiyuan Jia^{a,b}, Zhishui Yu^{a,b*}, Haichuan Shi^{a,b}, Shaowei Li^{a,b},
Di Wu^{a,b}, Hua Yan^{a,b}, Xin Ye^{a,b}, Jieshi Chen^{a,b}, Fuxin Wang^{a,b}, Yingtao Tian^d

^a School of Materials Engineering, Shanghai University of Engineering Science, Shanghai 201620, China

^b Shanghai Collaborative Innovation Center of Laser of Manufacturing Technology, Shanghai 201620, China

^c Fraunhofer Institute for Laser Technology ILT, Aachen 52074, Germany

^d Department of Engineering, Lancaster University, Bailrigg, Lancaster, LA1 4YW, United Kingdom

Abstract: There are mainly two kinds of laser used in welding of materials, continuous laser beam welding (CLBW) and pulsed laser beam welding (PLBW). The two kinds of laser welding have each welding characteristics. Compared with CLBW, the heat input of PLBW can be controlled lower, and has been widely used in the connection of thin plate materials. Since the pulse shaping can be edited to realize the preheating and slow cooling of each welding process, pulsed laser has been studied to suppress hot cracks and other defects in the field of aluminum alloy, magnesium alloy

* Corresponding authors: Dr. Peilei Zhang (peilei@sues.edu.cn), Dr. Zhishui Yu (yu_zhishui@163.com)

and other materials welding. This article describes the application of pulsed laser in alloy welding. The main welding problems and prevention methods were summarized. By discussing the index had been proposed to predict the sensitivity of solidification cracks, the formation and growth processes of hot cracks in pulsed laser welding was more comprehensively analyzed. Finally, the outlook for the future trends of pulsed laser welding is presented.

Keywords: Pulsed Laser; Welding; Crack criterion; Hot crack

Contents

1. Introduction.....	1
2. Pulsed laser	3
3. Characteristics of pulsed laser welding.....	6
3.1. Aluminum alloy	8
3.1.1 2××× (Al-Cu)	9
3.1.2 5××× (Al-Mg).....	10
3.1.3 Others	12
3.2. Nickel-based Superalloy	13
3.2.1 Hastelloy.....	13
3.2.2 Inconel.....	15
3.2.3 Others	16
3.3. Stainless steel	17
3.4. Magnesium alloy	19
3.5. Dissimilar welding	20
3.5.1. Al & Cu	20
3.5.2. Al & Steel.....	22
3.5.3. Others	23
3.6 Application of pulsed laser in hybrid welding.....	24

4. Prediction of hot cracking	26
4.1 Based on mechanical theory	26
4.2 Based on nonmechanical theory.....	28
4.3 Based on both mechanical and nonmechanical theory	31
5. Method for suppressing hot crack in pulsed laser welding	35
5.1. Phase composition and element diffusion.....	36
5.2. Microstructure evolution.....	39
5.3. Stress development.....	43
4. Summary and outlook	44
Acknowledgements	47
References	48

1. Introduction

The high-efficiency and high-precision welding features make laser applications more and more widely. In continuous wave lasers, welding parameters usually include laser power, welding speed, beam diameter, and defocus amount. However, pulse energy, pulse duration, and pulse frequency can also be regarded as parameters of pulsed lasers [1,2]. Pulsed laser welding can control welding heat input by adjusting several variables simultaneously [3], which make the laser processing of materials more flexibly. The interaction with materials during pulsed laser welding is also different from continuous laser. In addition to the simple summation of effect on each pulse, these results may also affect each other [4]. The overlap effect should be considered when defining the effective peak power density [5]. Pulsed laser has also many applications in hybrid welding, such as pulse-continuous wave double beam laser welding technology [6], and pulsed laser-arc hybrid welding [7–9].

For pulsed laser welding, weldable materials include aluminum alloy, superalloy, stainless steel, magnesium alloy and dissimilar metal materials. Because pulsed laser can meet precise heat input, it has great advantages in thin plate welding. The combination of low density and high strength make aluminum alloys more widely used in aircraft and vehicle manufacturing [10]. Dissimilar materials welding of aluminum and copper was used in many occasions [11–14]. The main defects of laser welding not only include pores, element evaporation and cracks, but also affect each other. For laser welding, Huang et al. [15] proposed two factors of pore formation: bubble formation caused by pore instability and bubble trapped at solidification interface. The porosity

can be restrained by preheating. The evaporation and diffusion of elements have an important influence on the welding process. In pulsed laser welding, Ti, B, Zr can reduce the solidification crack sensitivity of Al Zn Mg alloy [16]. Kim and Nam [17] studied the effect of transition elements Mn and Zr on the crack sensitivity of 7000 series high strength Al-Zn-Mg alloy welding, while Cu and Cr increased the crack sensitivity. Holzer et al. [18] measured the change of weld element concentration by EDS, and calculated the solidification zone by using these quantitative data. Their study proved that the energy of per unit length of AA 7075 laser welding can cause the change of weld element concentration, thus affecting the hot cracking sensitivity.

Due to the use of solid solution and precipitation hardening heat treatments, superalloys generally exhibit a combination of enhanced mechanical strength, creep fracture performance and resistance to environmental erosion (including oxidation) at operating temperatures close to melting points [19]. The weldability of heat-resistant nickel-based superalloys become more important, because welding is widely used to manufacture and repair hot-segment components of aviation and industrial gas turbine engines made by these materials [20–22]. Unlike the solidification cracks of aluminum alloys, liquefaction is the main cause of heat affected zone (HAZ) crack in most austenitic alloys (including precipitation hardened Ni-based superalloys) [23]. Many studies had shown that the conventional pulsed laser welding method is not obvious in solving the liquefaction cracks of superalloys [24–26].

Magnesium (Mg) alloy has the advantages of high specific strength, specific rigidity and shock absorption. Using Mg alloy instead of aluminum alloy can reduce

the weight by 15%-20% [27]. Porosity and crack are common defects of magnesium alloy welding, studies have shown that they can be solved by the characteristics of pulse overlap and editing pulse shaping [28–30].

In order to deepen the understanding of the pulsed laser welding process, it is necessary to compare the results of pulsed laser welding of different materials. After reviewing these studies, it was found that there are many problems in pulsed laser welding, and cracks as the most common defects in welding attract the attention of many researchers. Therefore, many indexes have also been proposed to predict the thermal cracking sensitivity of solidification process. However, especially for the rapid cooling of pulsed laser welding, most of the crack sensitivity indexes are not applicable. In this review, through a comprehensive analysis of the mechanism of thermal crack generation, researchers could fully understand the formation of thermal cracks in the process of pulsed laser welding, and the use of pulse methods to solve laser welding problems of alloy.

2. Pulsed laser

Laser welding is a fusion welding technique, which is achieved by focusing the laser beam to a very thin spot and obtaining a very high power density, A laser power transmission model built in conformity with the ray tracing scheme is proposed [31], as shown in the Fig.1. The focusing conditions of the laser beam affect keyhole behavior and energy density distribution on the material, therefore are also important factors affecting the energy absorption mechanism of the plasma plume. In the heat conduction welding mode, a strong plasma plume is usually generated. The effective absorption of

laser energy by the material is shielded. The small keyhole behavior helps to improve the absorption efficiency of plasma and laser energy. Once the energy density of the laser beam is sufficient to produce the keyhole, the plasma's reverse toughening radiation absorption effect will be weakened [32].

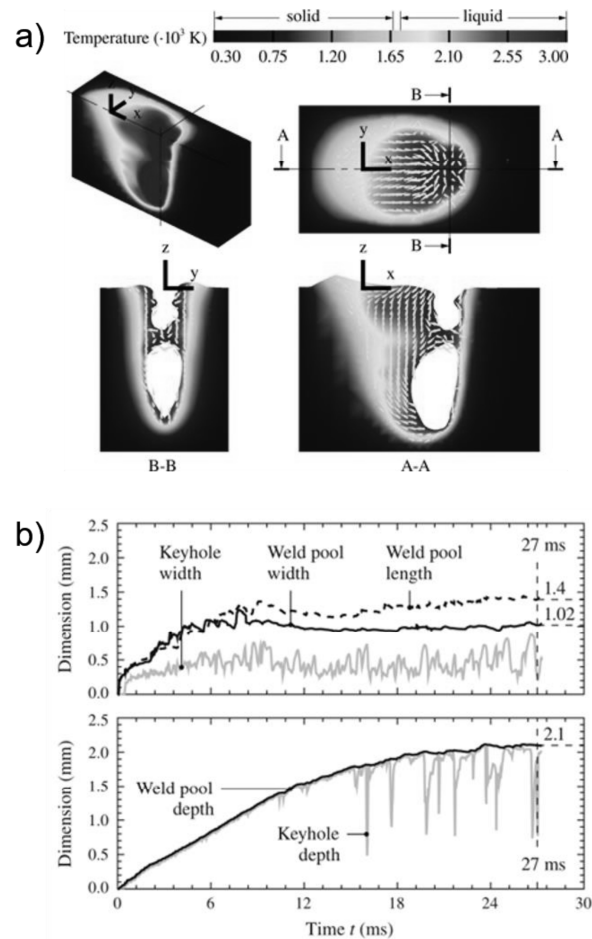


Fig.1. a) Calculated weld pool geometry after 27 ms of welding time; b) Calculated length, width (top) and depth (bottom) of the weld pool and keyhole [31].

Pulsed laser welding can perform spot welding or continuous seam welding with overlapping welded spot. When low heat input is required, pulsed laser welding is mainly used [33]. Pulsed laser welding can be seen as a series of spot welds. Liang and Luo [34] established a three-transient numerical model of pulsed laser welding of dissimilar metals, and found that the surface ripples are mainly caused by periodic laser

and molten pool solidification. The higher pulse overlap factor, causing the lower the solidification rate, the more uniform the penetration and the finer the ripples, as shown in the Fig.2. Pulse shaping plays an important role in controlling welding defects of materials, which is usually used for welding thin-plate shells and other components. Bertrand and Poulon-Quintin [35] studied the use of pulsed laser for the welding of dental alloy Co-Cr-Mo and Pd-Ag-Sn cast plates for denture restoration. Slow cooling ramps can be used to better control the solidification process and always prevent internal defects. Because Co-Cr-Mo alloy has a low laser beam reflectivity, the fast slope should be preferred. In contrast, for the Pd-Ag-Sn alloy, since the alloy has a high laser beam reflectivity, the slope that rises slowly should be selected.

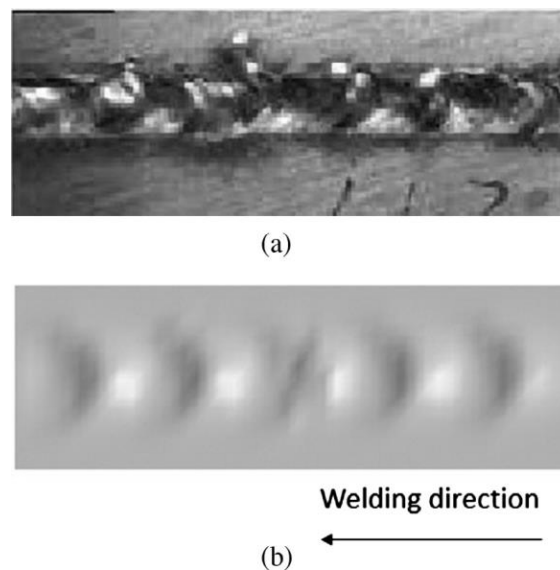


Fig.2. (a) Comparison of experimental; (b) simulated weld bead geometry in similar welding [34].

Pulsed laser is not only used for welding materials, but also have many applications as auxiliary welding or surface treatment before alloy welding. The welding quality can be improved by removing filth and oxide film on the surface of

aluminum alloy. Experiments showed that cleaning the surface of the welding workpiece by picosecond laser is better than nanosecond laser [36]. Alshaer et al. [37] found that nanosecond pulsed Nd: YAG laser cleaning significantly reduced the porosity of AA6014 weld. This was due to the elimination of pollutants and oxide layers, which contributed to the formation of porosity. Laser cleaning is based on thermal ablation. Banat et al. [38] developed a miniature laser scratching process based on the latest generation of nanosecond pulsed laser, the interaction between laser and materials in ultra-thin aluminum foil (thickness is 160 μm) was observed. Microscopic surface cleaned by pulsed laser with different overlap ratio is shown in Fig.3.

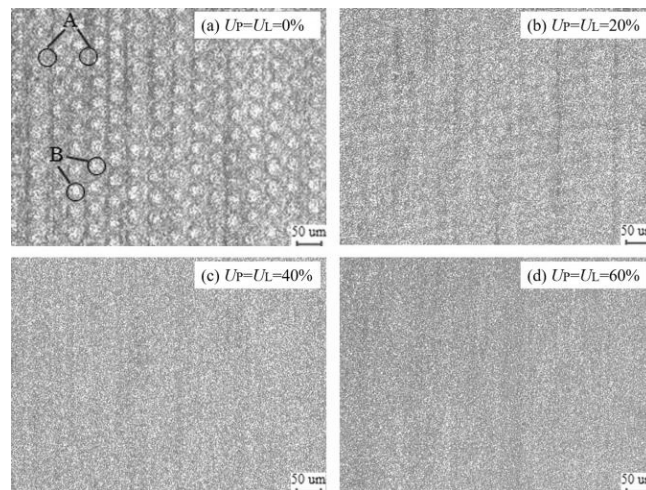


Fig.3. Micromorphology of aluminium alloy surface cleaned with different overlap ratio by picosecond laser [37].

3. Characteristics of pulsed laser welding

In the laser welding process, the state of the keyhole has an important influence on the welding process, including: vapor plume, porosity and spatter. Therefore, the study of keyholes in laser welding process is important, researchers have proposed many methods for studying keyholes. Based on the butt joint structure made of

transparent glass and stainless steel, it observed the dynamic keyhole profile of high-power laser welding, and study the effect of vapor pressure in the keyhole on plasma and spatter [39,40]. With the development of infrared technology, it can not only be used to detect weld penetration, weld surface quality[41], the application of infrared sensing technology to extract thermal gradient parameters based on the heat distribution of the molten pool can be used to determine the deviation between the laser focus and the center of weld [42]. In past research, chromatic filtering of the thermal radiation from a weld pool is used to detect power changes and focus shift [43]. Researchers had developed a sensor that measuring plasma temperature, and thus weld penetration depth and defects can be detected synchronously [44]. As an emerging detection technology applied in the welding process, acoustic emission (AE) technology can be used to characterize the behavior of the plasma plume in pulsed laser welding [45], as shown in the Fig.4.

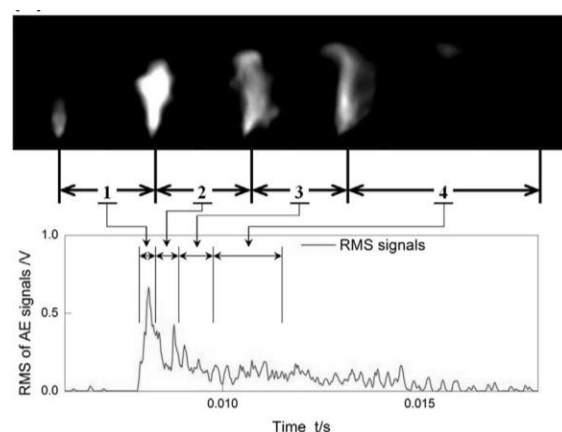


Fig.4. Development of plasma plume and corresponding AE signals [45].

Numerical simulation is also an important method to study the dynamic welding process. Considering effects of phase transition, recoil pressure, thermo-capillary, natural convection, vaporization and temperature dependent material properties, a heat

source model for pulsed laser spot welding describing the reflection of multiple beams in the keyhole has been developed [46], as is shown in the Fig.5. Numerical simulation can also be used to study the influence of recoil pressure, solidification and vaporization on the dynamics of the molten pool and weld formation in pulsed laser welding [34].

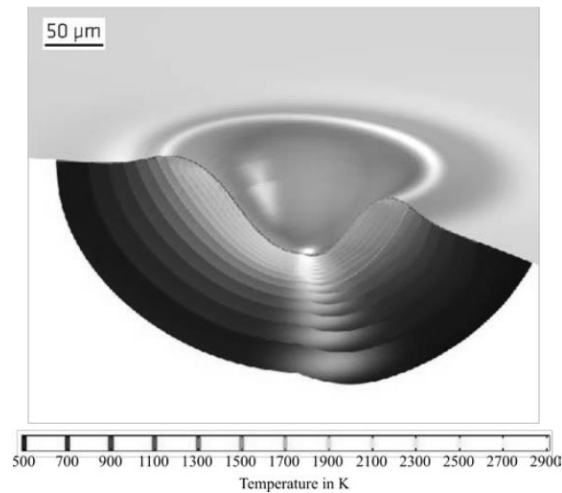


Fig.5. Rotational extruded simulation results at 1.2 ms - the time of maximum elongation of the weld pool [46].

Real-time detection and signal acquisition of defects in the laser welding process are hot issues. Using the high-speed camera to observe the dynamics of the keyhole and molten pool through the glass, it can directly reveal the mechanism of pore formation [47]. In order to better understand the solidification and crack formation in laser manufacturing. A special experimental device with a high-speed camera can be used to measure the strain during the welding process, and determine the critical strain required for the formation of solidification cracks [48]. In the study of M. Miyagi [49], the internal characteristics of crack propagation of aluminum alloy in laser spot welding were directly observed by X-ray phase contrast method.

3.1. Aluminum alloy

Aluminum alloy has become an important structural material due to its high weight ratio. While due to high reflectivity and high sensitivity to hole and thermal cracking, high-strength aluminum alloys are difficult to weld, it also has high application potential in the lightweight structure of the automotive industry. So, it is necessary to improve the weldability of aluminum alloy. The main problem is the high thermal cracking sensitivity. Aluminum alloy welding has high thermal energy characteristics, requires a high energy density power source, high thermal expansion, high solubility of hydrogen and nitrogen during the fusion welding process, resulting in increased porosity, incomplete penetration of aluminum oxide film Al_2O_3 , surface tension or viscosity inferior and therefore challenging. Different series of aluminum alloys have different crack sensitivity. On the basis of two-dimensional phase field simulation, Geng et al. [50] demonstrated that Al-Mg alloy has better resistance to solidification cracking than Al-Cu alloy in a wider solidification temperature range.

3.1.1 2xxx (Al-Cu)

Al-Cu series aluminum alloys generally have high crack sensitivity. Aluminum alloy AA2219 can be used to manufacture the propellant cabin of launch vehicle. It is proposed that under certain conditions, such as improper fixtures, large heat input, and large material grain size, cracks may occur [51]. Ahn et al. [52] used fiber laser to weld the crack-sensitive 2024 aluminum alloy. Bead welding of 2024-T3 plates with a thickness of 3 mm was carried out, it was found that the addition of filler metals with different chemical compositions can narrow the crack sensitivity range. Ghaini et al. [53]'s experiment involved Nd: YAG pulsed laser welding of 2024 aluminum alloy, it

proposed that liquefaction cracks are strong initiation points of solidification cracks. Repairing the liquefaction grain boundary by backfilling plays an important role in resisting liquefaction cracking in the partial melting zone, which in turn affects the solidification cracking tendency. Based on the assumption of mass conservation, Sheikhi et al. [54] used a model to predict the conditions of solidification cracks in 2024 aluminum alloy pulsed laser welding. The model proposed that in order to avoid solidification cracks, the corresponding solidification rate should be reduced as the length of the vulnerable area increases. By appropriately controlling the shape of the ramp-down pulse, solidification cracks can be avoided. The model proposed by Sheikhi et al. can also predict the effect of initial temperature of base metal on crack sensitivity. The numerical model is shown in the Fig.6.

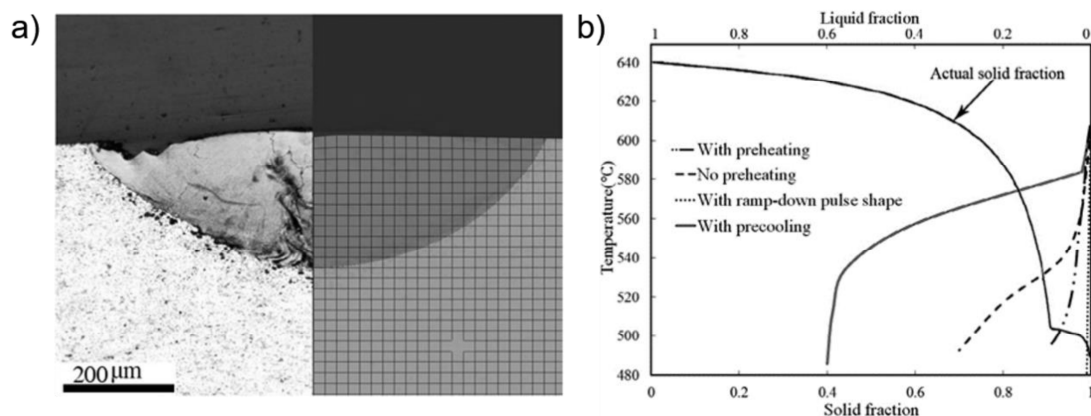


Fig.6. a) The comparison of experimental and calculated weld pool shapes for pre-cooled sample; b) Superposition of the actual solidification path of alloy AA2024 and the maximum allowable solid fractions to avoid solidification cracking for different welding conditions [54].

3.1.2 5××× (Al-Mg)

When using dual lasers including Nd: YAG and diode with beam spacing of zero

to weld 0.05 mm AA5052H19 thin plate to improve absorption characteristics of the beam, greater melting and better surface quality can be obtained through preheating [55]. Workpiece could also be preheated by pulse shaping of pulsed laser. For AlMg4.5 alloy foils with thicknesses of 0.2 mm and 1 mm, respectively, Rohde et al. [56] implement pulse shaping through combining three rectangular pulses with different durations and power levels. Welding mainly occurs in the second phase pulse waveform, the first pulse is used to preheat the sample, while the third pulse controls the molten pool behavior. This process can be used to control aspect ratio of the weld and improve surface quality. ABIOYE et al. [57] performed pulsed laser welding of AA5052-H32 with a thickness of 0.6 mm. The welded joint formed under the lower heat energy input exhibits a fine dendritic grain structure. The vaporization of Mg element and formation of hard phase compounds ($Al_{10.5}Fe_3Si_{0.5}$) are reduced. Li et al. [58] studied the influence of oscillation parameters on the weld porosity and morphology of 5083 aluminum alloy plates. Laser beam oscillation can refine the grains and promote the β (Mg_2Al_3) phase in the weld fusion zone Evenly distributed, and because the generation of pores is suppressed, the tensile properties are significantly improved.

Thermal cracking of aluminum alloys in pulsed lasers can be avoided by preheating. Moreover, increasing average laser power and pulse frequency greatly reduce the thermal cracking tendency, reducing the pulse duration also has the same effect [59]. Beiranvand et al. [60]'s calculation of 5083 aluminum alloy shows that when the laser pulse frequency is increased, the thermal cracking sensitivity is reduced. At the same time, the continuous evaporation of Mg increases the thermal crack

sensitivity, however, the solidification rate effect on the crack sensitivity is more obvious than the Mg content.

3.1.3 Others

In terms of base material, the decrease in the hardness of weld metal is mainly due to the evaporation of the Mg element during the laser welding process. It has been found that pulse shaping with the same pulse energy but different combinations of peak power and pulse duration will produce different results. Ramp-down pulse shaping and ramp-down with longer initial coupling provide the best welding quality [61]. Jun et al. [62] proposed a pulsed laser welding formula for 2mm thick TiB₂ reinforced aluminum matrix composites. When the parameters satisfy the formula $f = (3.6-5.4) v$, a good welding effect can be obtained, where v is the welding speed and f is the laser pulse frequency. Through real-time monitoring of the welding process, using the adaptive control of laser pulse, it significantly improved the defects and strength of aluminum alloy welded joints [63].

From a hot cracking perspective of aluminum alloys 6061, 5456, and 5086. Cieslak and Fuerschbach [64] observed that pulsed Nd: YAG laser welds are extremely susceptible to thermal cracking of the weld metal, while continuous wave Nd: YAG laser welds are no crack. At higher interface speeds, the strain rate is the main cause of thermal cracking; at lower interface speeds, thermal cracking is caused by the large amount of hydrogen diffusion on the solid-liquid interface [65]. If the rectangular pulse is modified into three stages with different power, it can make the molten pool absorb more energy and reduce the cooling rate, to a certain extent, it can also prevent

evaporation, Fig.7 shows the change of the surface temperature of the molten pool due to the pulse shaping modulated [66].

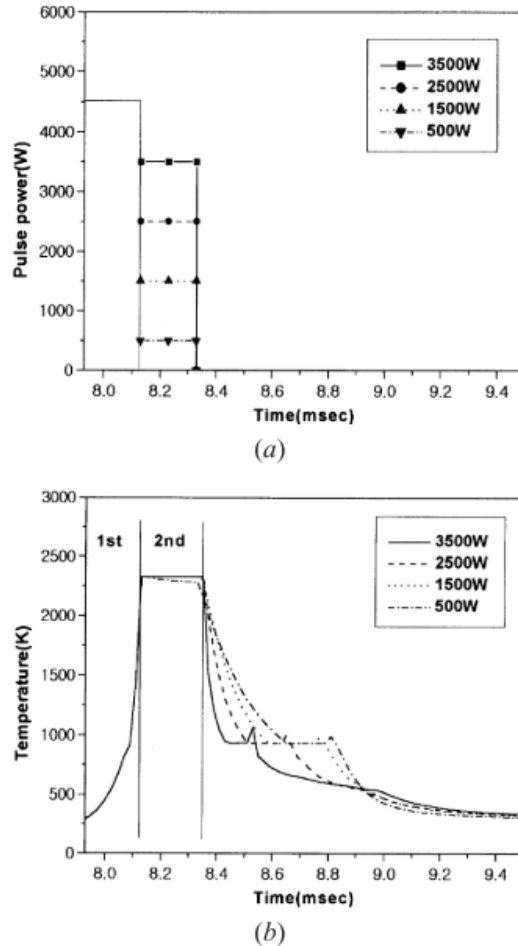


Fig.7. Effect of pulse waveform on surface temperature of molten pool [66].

3.2. Nickel-based Superalloy

3.2.1 Hastelloy

Solidification cracks are caused by liquefaction cracks in the heat affected zone of base metal and propagate along the grain boundary of the welded metal. Using tailing pulse can obtain proper cooling rate to reduce the residual stress and deformation of Hastelloy C-276 sheet laser welding [67]. Ma et al. [68] found elemental segregation in the pulsed laser welding of Ni-based Hastelloy C-276, the tendency of brittle phase

formation weakened. Dislocation accumulation is the main reason for the decrease in tensile strength. In the study of Shanthos Kumar et al. [69], the effect of welding speed on tensile strength on laser welding of Hastelloy C-276 and Monel 400 alloy plates is the greatest, while the influence of pulse energy and pulse width on tensile properties is smaller. By optimizing the process parameters, an empirical formula for predicting mechanical property was established. Pakniat et al. [24] found that the use of pulsed lasers formed thermal cracks in the weld, but thermal cracks did not occur in the continuous wave lasers welding, the result is shown in Fig.8. Increased laser pulse frequency and pulse duration can reduce the tendency of thermal cracking.

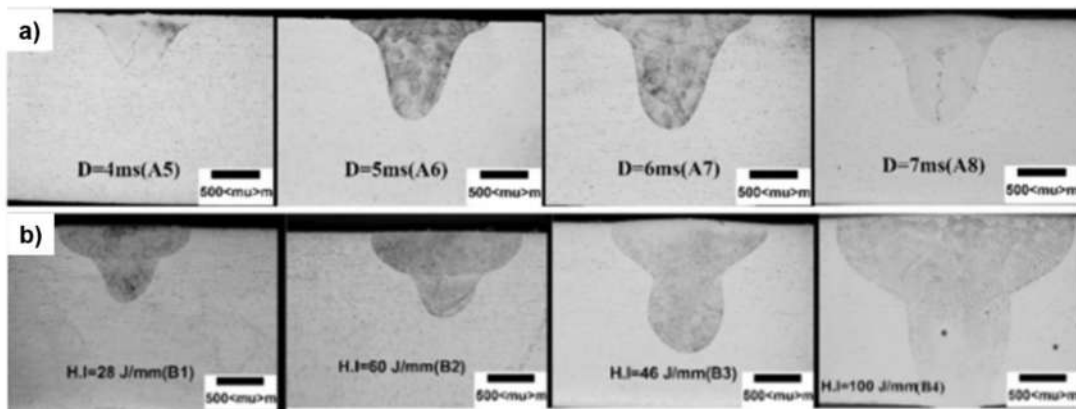


Fig.8. Avoid thermal cracks by using continuous wave lasers instead of pulse wave laser: a) Pulse wave laser; b) continuous wave laser [24].

In the laser welding process of Hastelloy C-276, welding speed, pulse energy and frequency all have effects on the aspect ratio and peak temperature of weld [70], as shown in the Fig.9, combined with numerical simulation, the best parameters can be obtained. Azimzadegan and Akbari Mousavi [25] modeled the thermodynamics of the weld and found that the location of the liquefaction cracks depended on the evolution of the microstructure of the precipitates, which is determined by the temperature and

stress distribution in the Hastelloy X laser weld, Fig.10 shows the microstructure of the heat affected zone of the Hastelloy X.

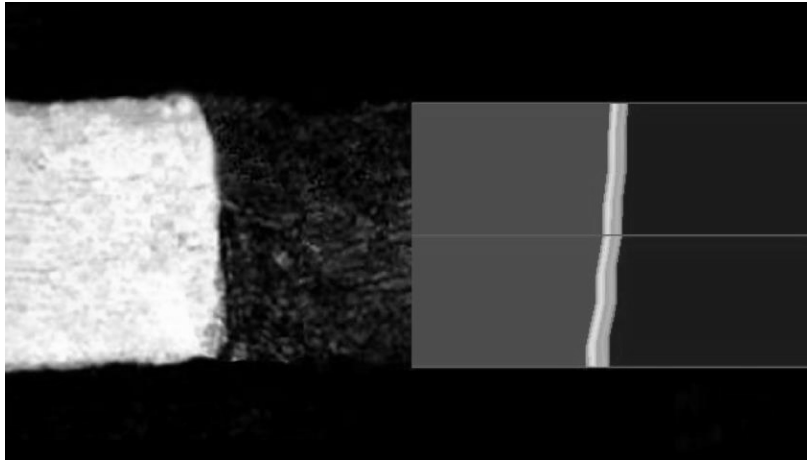


Fig.9. Macrograph of the weld bead and results of numerical simulation [70].

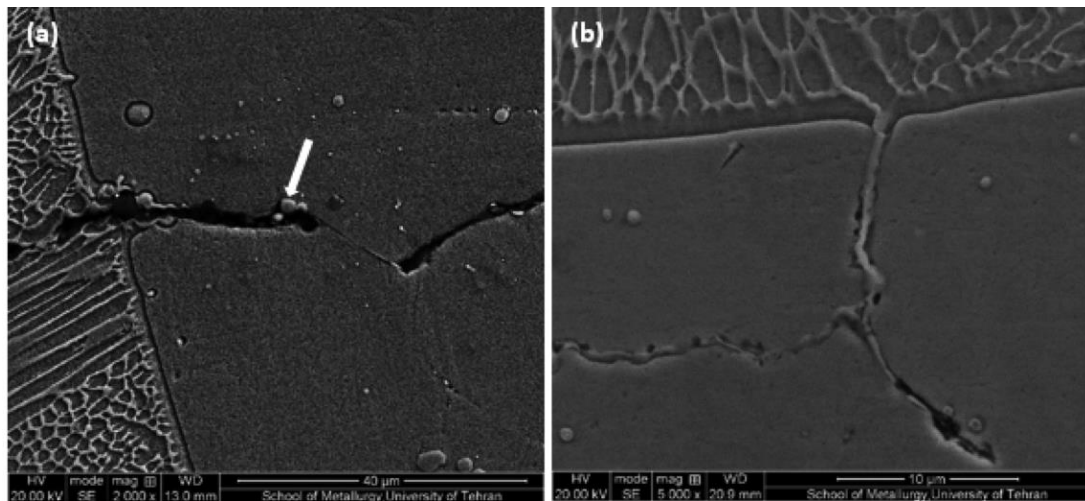


Fig.10. SEM micrograph: a) liquefaction cracking; b) backfill of liquefaction [25].

3.2.2 Inconel

The main strengthening phase of 738 superalloy has a large amount of liquefaction after heat treatment before welding, which has a significant effect on the liquefaction of grain boundaries in the heat affected zone and the cracks it generates [23]. Fig.11 and Fig.12 show the effect of intragranular particles of heat affected zone on Liquid film from liquated interface. Montazeri and Ghaini [71] used pre-weld heat treatment

to explore the liquefaction cracking behavior of low-power pulsed laser welding of IN738LC. The results show that the liquefaction cracks in the alloy are mainly related to γ - γ' eutectic, MC carbide, Cr-Mo boride and Ni-Zr intermetallic.

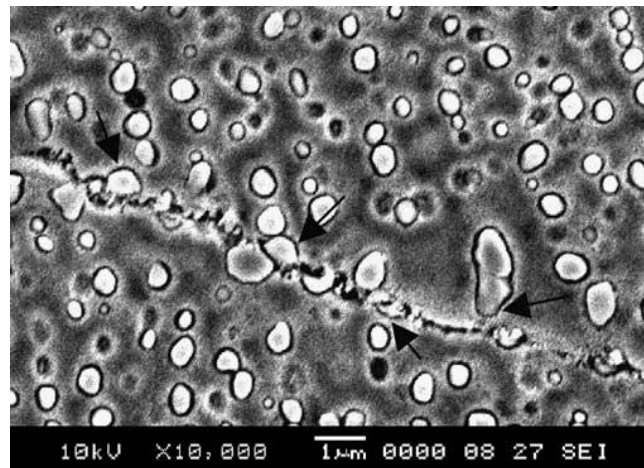


Fig.11. Liquid film formed by liquefaction of particle boundary at HAZ [23].

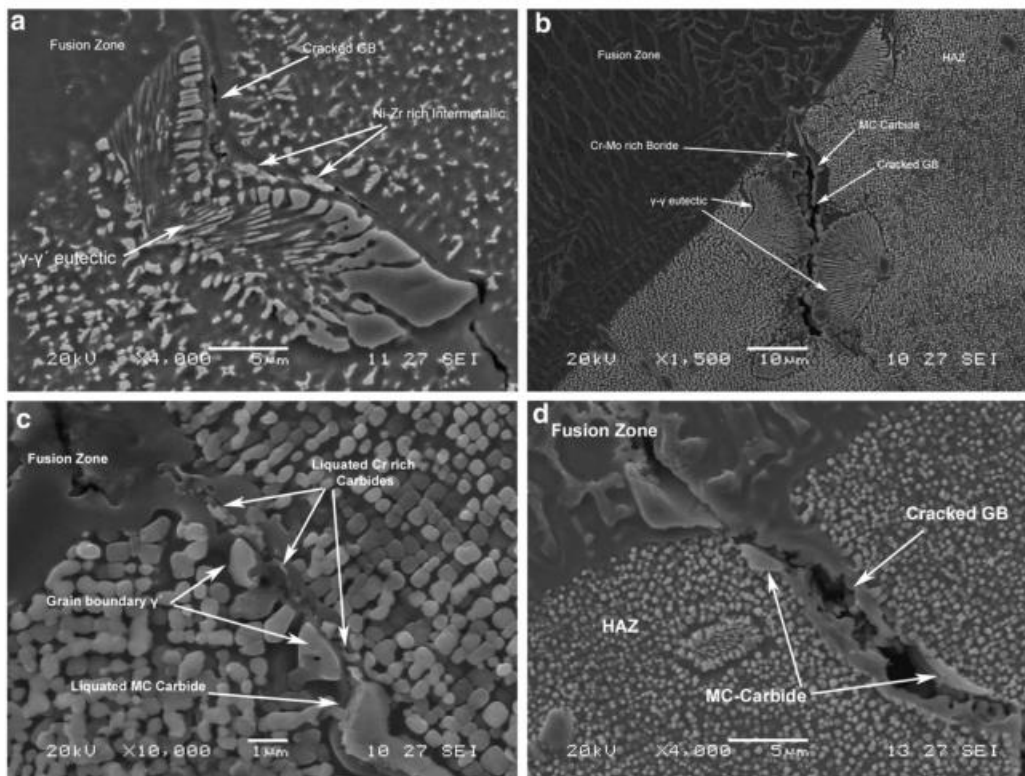


Fig.12. Intermetallic, boride and carbides resulting in HAZ liquation cracks [71].

3.2.3 Others

In the pulsed laser welding process, the liquefaction cracks in GTD-111 nickel-based cast superalloys are related to the melting of γ particles, MC carbides, interdendritic γ - γ' eutectic and Cr-rich boride. Cracks are also prone to occur where Al and Ti are highly concentrated [26]. The peak welding temperature of Monel 400 alloy sheet, the width of the weld and the size of the heat affected zone increase with the increase of pulse energy. With a pulse energy of 10 J, the maximum hardness and tensile strength can be obtained [72]. Jiang et al. [73] compared pulse wave and continuous wave laser welding of GH3535 superalloy. The grain size of the pulse wave joint is smaller than the grain size of the continuous wave joint, and the molten pool oscillation effect of which reduces the generation of pores.

3.3. Stainless steel

The weldability of stainless steel is better than that of aluminum alloys and high-temperature alloys, and thermal cracking is generally rare in laser welding. Compared with high-heat input pulses, low-heat input pulses can usually produce fine-grained structures and improve mechanical properties, regardless of the composition of the base material [74]. When welding AISI 409 stainless steel by pulsed laser, when laser energy density is more than 4 GW/m^2 , the mode changes from thermal conductivity welding to deep penetration welding [75]. Meng et al. [76] uses pulsed laser to weld AISI 405 and AISI 321 dissimilar stainless steel plates. Frequency is the most important factor affecting the weld penetration, the pulse shaping and back groove have a great effect on the porosity. Through a three-dimensional model based on FEA, Jayanthi et al. [77] studied the conduction and convection heat transfer in the welding process of AISI 316L

stainless steel sheet by pulsed Nd:YAG laser welding. The influence of pulse frequency and peak power are more significant than that of pulse width and welding speed. By optimizing parameters, the tensile strength can be close to 96% of the base metal [78]. Multi-wavelength pyrometers and filters can be used to measure the temperature change of the molten pool during 304 stainless steel pulsed laser welding. In order to avoid thermal decomposition of certain melt compounds, it is necessary to apply a higher energy density flux at the beginning of the laser pulse [79]. Saravanan et al. [80] changed the welding heat input by changing the welding speed and found that a higher volume percentage of ferrite affects the phase balance of the base alloy. The phase imbalance of laser welding can be alleviated by post-weld heat treatment, in order to improve corrosion performance of laser welding. Bahrami Balajaddeh and Naffakh-Moosavy [81] studied the effect of pulsed laser welding high cooling rate on the crack resistance of 17-4 martensitic precipitation hardening (PH) stainless steel (SS). The welding parameter that most affects 316 stainless steel undercut defects is power, followed by pulse width and frequency [82]. When reducing the overlap rate in pulse laser welding can achieve extremely high cooling rates, the transformation of ferrite to austenite in the duplex stainless-steel weld can only be limited to the grain boundary [83]. The weld metal of austenitic stainless-steel pulsed laser welding undergoes multiple melting and solidification, which is sensitive to power level and scanning speed. In addition, the dual-phase austenite/ferrite structure, recrystallized structure and high dislocation density in the fusion zone were observed in the pulse overlap region [84].

Laser power is the most important parameter for high-quality welding of stainless steel sheet. Pulse overlap will seriously affect the surface integrity (surface roughness) and strength of the welded joint. Due to the different cooling rates, the microhardness of the heat affected zone is lower than that of the welded metal, and laser pulse energy has a significant effect on the residual stress of the welded joint [85]. Welding deformation is the problem of ultra-thin stainless-steel plate welding. Xu et al. [86] welded 316L stainless steel with 0.07mm thickness, it is found that the deformation of the specimen is convex when the input energy is low. However, with the increase of input power, the deformation tends to be concave. With the decrease of incident angle, the shape of weld pool changes from hemispherical or near spherical to teardrop. At the same time, the microstructure of the weld is also affected by the angle of incidence, plane dendrite, fine columnar dendrite and coarse columnar dendrite were observed at the incident angles of 89.7°, 85.5° and 83°, respectively. The carbide and δ ferrite precipitation rates of austenite matrix were higher at the incident angles of 85.5° [87].

3.4. Magnesium alloy

Porosity is a common defect of magnesium alloy welding. Chen et al. [28]'s experiments show the pores of welded joint are usually located at the bottom of the fusion zone of the welded joint, then larger depths are more likely to cause pores. Pore generation can be reduced by overlapping of adjacent pulsed laser. The effect of Overlap rate on porosity is shown in Fig.13. Their study also used the pulsed laser-arc hybrid welding in magnesium alloy. Compared with the negative waveform, while the pulsed laser acts on the positive waveform of the arc discharge, a better-quality weld

could be obtained. In this way, the laser action spot limits the position of the arc plasma discharge on the workpiece to increase the arc energy density of the welding [88].

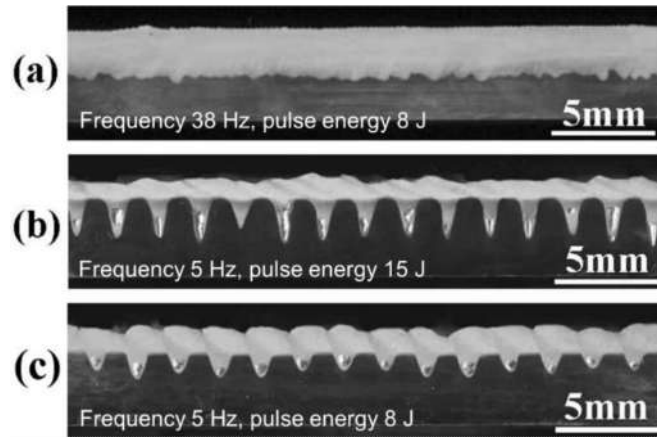


Fig.13. The effects of different laser pulse overlap rate on porosity state [88].

Increasing the peak power of pulsed laser during slow cooling will reduce the sensitivity to solidification cracks, but too high will cause the crack sensitivity to increase again due to the higher thermal and shrinkage stresses. Under the same pulse energy, the coupling effect of the ramp pulse is better than leading spike pulse and rectangular pulse [30].

3.5. Dissimilar welding

3.5.1. Al & Cu

The heat input of pulse welding has an important influence on the formation of intermetallic compounds (IMC), which in turn affects the mechanical properties of the welding joints. Fig.14 shows that laser heat input has an important effect on the static shear strength and cyclic shear strength of Al-Cu joints [12]. At a constant pulse energy, as the distance between pulses increases shown in the Fig.15, the maximum stretching of the Al-Cu joint increases first and then decreases. The maximum tensile load obtained with the preheated pulse shape is higher than its corresponding slow cooling

pulse shape [14]. With increasing of laser power, the shear strength of The Al/Cu joint increases and then decreases, and the weld metal is mainly composed of solid solution (Al) and Al-Cu cocrystal line alloy, and the fracture occurs mainly in the Al-Cu cocrystal line region, which has the characteristics of brittle fracture [11].

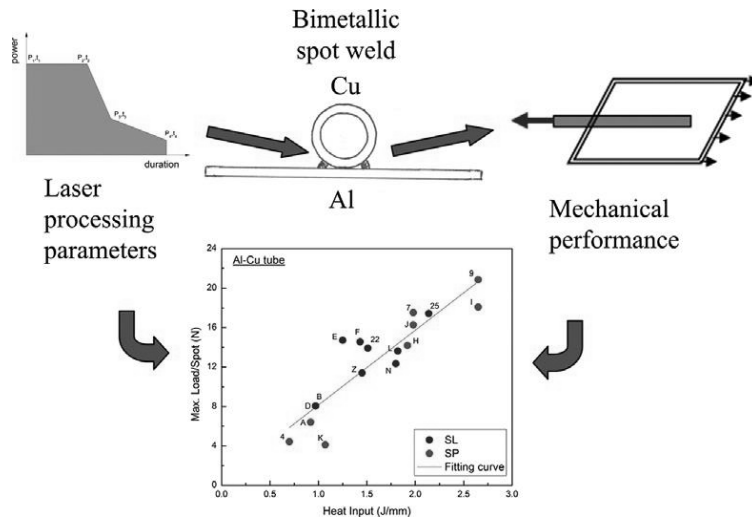


Fig.14. Effect of heat input on maximum shear load of Al-Cu tube system [12].

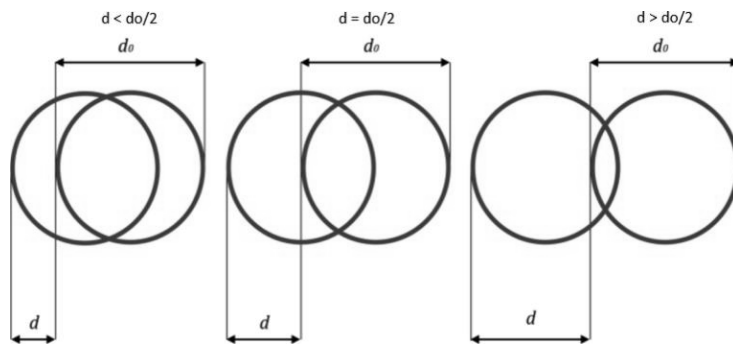


Fig.15. Schematic diagram of pulse distance [14].

Dissimilar joints of Al and Cu are often used in electrical engineering. However, the formation of brittle intermetallic compounds makes the welding of dissimilar metals involve many challenges, the high reflectivity and poor solderability between materials also hinder the application of Al and Cu dissimilar welding. Applying different pulse shaping to oscillate the molten pool could make the aluminum-copper mixture in the

weld more uniform [89], the optimized pulse shaping is shown in Fig.16(b). In Mathivanan and Plapper [13]'s study, the wide distribution of brittle metal-to-metal compounds improved the ductility of joints through beam oscillation. The presence of a discontinuous interface facilitates mechanical resistance. Pulse shaping with warm-up, welding and cooling stages help improve shear strength and reduce porosity. The oscillation mode and pulse shaping are shown in Fig.17.

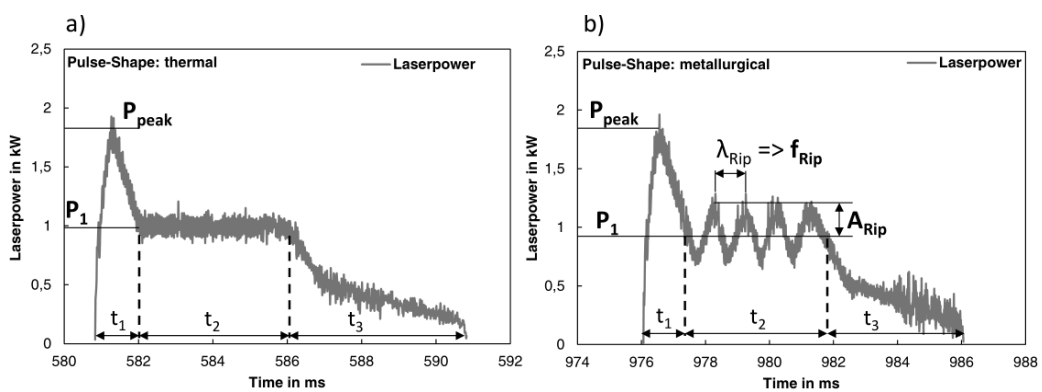


Fig.16. Shape-parameters of a thermal optimized pulse (a) and a metallurgical optimized pulse (b) [89].

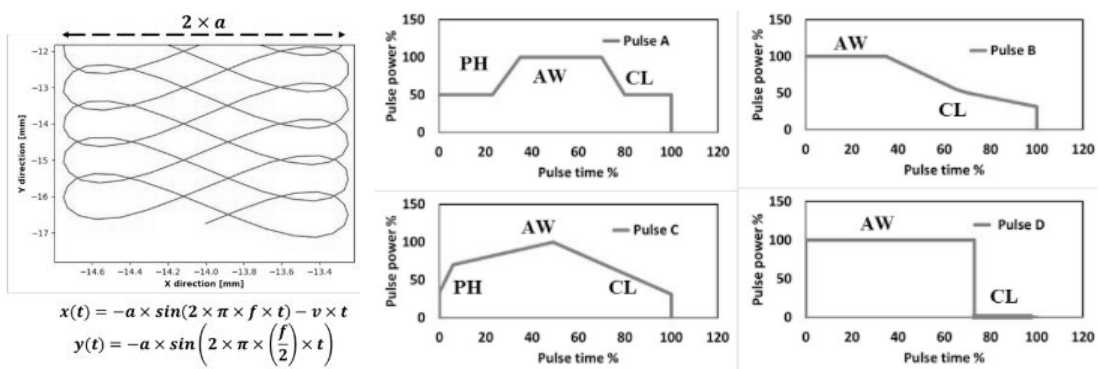


Fig.17. (a) Spatial beam oscillation (Infinite shape) in x and y direction; (b) Profiles of the pulse [13].

3.5.2. Al & Steel

Intermetallic compound is also the main problem of dissimilar welding of aluminum and steel. For pulsed laser welding, the percentage of intermetallic

compounds in a welded joint depends on three factors: Increasing peak power with a fixed pulse energy, increasing pulse duration with a fixed peak power and increasing overlap factor with a fixed pulse energy and peak power [90]. Li et al. [91] systematically analyzed the effects of IMC on steel/aluminum welding using the first principle method. Fe_3Al and FeAl_2 have plastic properties; FeAl , Fe_2Al_5 , FeAl_3 and $\text{Fe}_4\text{Al}_{13}$ exhibit brittle characteristics; FeAl binary compounds have typical metal properties. Lower laser energy density has a significant effect on reducing the formation of intermetallic phases. And at relatively low laser energy density (1250 J/mm^2), the welding interface has the lowest defects such as cracks [92].

The mechanical properties of the laser joint are closely related to the depth of the weld. In high melting depth ($354\mu\text{m}$) joints, Fe-Al IMCs with microcracks are formed at the Al/fusion zone interface, in low melting depth ($108\mu\text{m}$) joints, a non-defective iron-based IMC is formed at the Al/fusion zone interface [93]. Indhu et al. [94] used a high-power diode laser to connect 6061 aluminum and dual-phase (dp600) steel in pulsed mode. The metal phase (Fe_2Al and FeAl_3) is formed in a smaller thickness with the range of $1\text{-}7\mu\text{m}$.

3.5.3. Others

In CP Ti and stainless steel plates welding with pulsed Nd:YAG laser, the ramp-down pulse shaping showed in Fig.18 reduces the mixing between the two welding materials in the weld, thereby reducing the formation of intermetallic phases and the welding strength of the ramp-down shaping is higher [95].

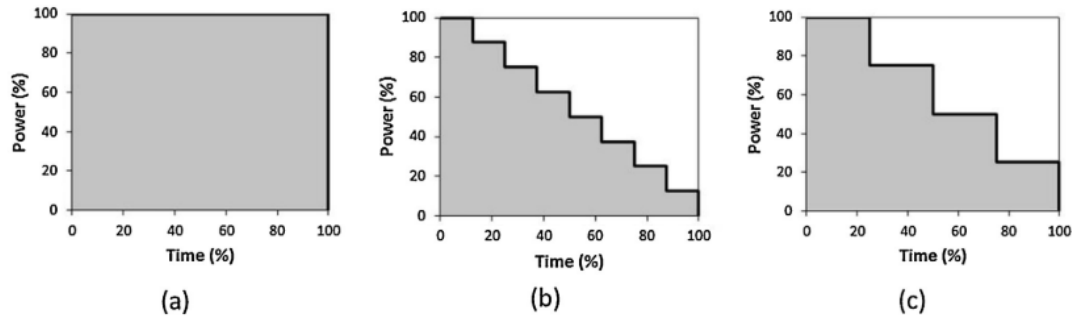


Fig.18. Pulsed wave used in CP Ti and stainless steel plates laser welding [95].

In pulsed laser welding, because of rapid cooling, the distribution of elements in the weld will be uneven [96]. Adding intermediate layer to limiting defects of dissimilar materials welding is also a feasible method. In Zhang et al. [97]'s work, the formation of these brittle Ti Fe intermetallic compounds is prevented by copper as an intermediate layer when titanium alloy is connected to stainless steel (SS). Fang et al. [98] inserted Cu/Nb double layer to welded TC4 and AISI 316L, even if the laser power is low, the suppression of cracks is not obvious. The kovar alloy can be used as the intermediate material between glass and AISI 304L, the increase of heat input results in the increase of thermal stress, which leads to the generation of cracks [99].

3.6 Application of pulsed laser in hybrid welding

For the application of automated welding technology, it is necessary to reduce defects in welding and increase welding manufacturing speed. The distance between the laser beam axis and the tip of the GTAW electrode will seriously affect the stability of the welding process [100]. In the 5mm thick 5083 aluminum alloy pulsed laser-MIG hybrid welding, the rear MIG can improve the stability of the keyhole and decrease the porosity [101]. Fig.19 shows the effect of separation distance and MIG torch direction.

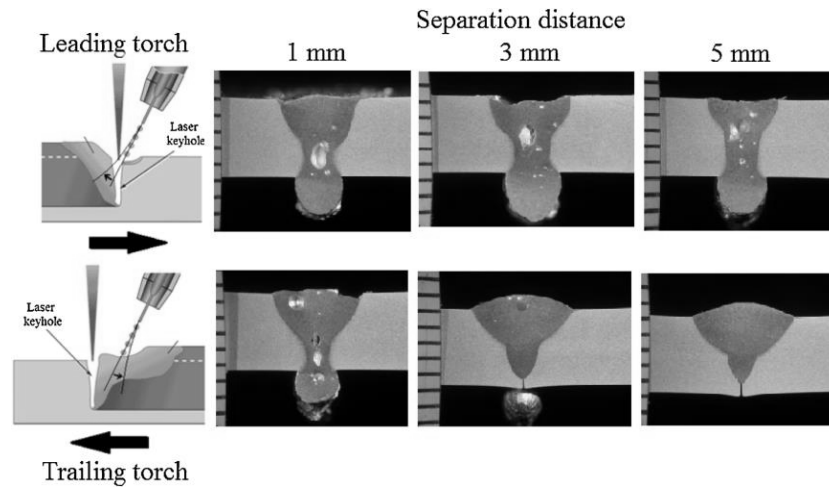


Fig.19. The effect of separation distance on weld appearance and quality in fiber laser-MIG hybrid welding of AA5083 [101].

Using pulsed laser to induce TIG welding could reduce the loss of weld element and porosity [102]. For laser and arc welding that also has pulsed characteristics, when the pulsed laser irradiated the solid-liquid interface of MIG welding droplets, Jia et al. [9] found that the laser as an additional separation force significantly increased the stability of the welding process; by changing the stress state of the droplets, the short circuit transfer and spray transfer were promoted welding process, effectively increasing the transfer frequency. As shown in Fig.20, compared with in-phase laser MIG hybrid welding, the inverse laser-MIG waveform composite welding has greater penetration, less weld spatter, less porosity, and improved tensile properties [7].

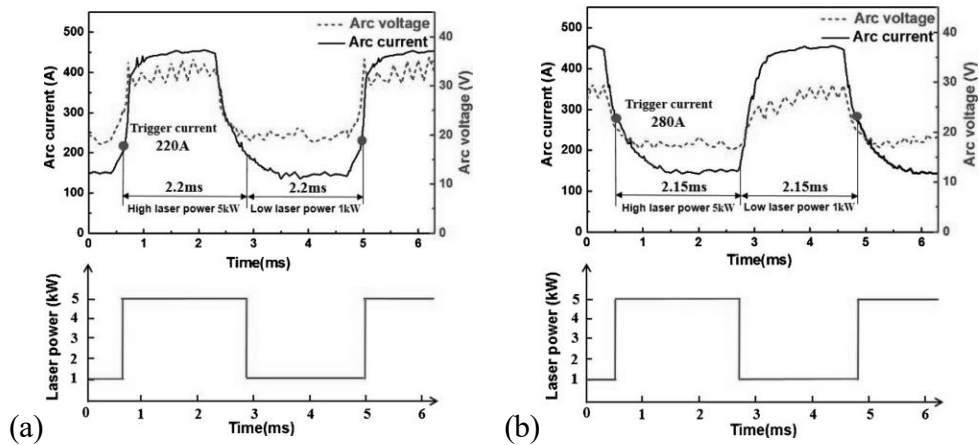


Fig.20. The waveforms of in-phase(a) and anti-phase(b) laser-MIG synchronized pulse modulations [7].

4. Prediction of hot cracking

Solidification cracks, also known as hot cracks in castings, are intergranular or dendritic cracks that occur under limited solidification conditions. Casting and welding are common examples where there are limited solidification conditions. Solidification cracking usually involves the presence of a liquid film at the grain boundaries of the melting zone. The liquid film may also exist in the heat affected zone or partially melted zone, and may cause another form of rupture, called liquefaction rupture. Most of the crack sensitivity models proposed at present are derived from casting theory, and can be divided into three theories according to the mechanism: based on mechanical theory, based on nonmechanical theory and based on both mechanical and nonmechanical theory. There have been a few studies to modify some of these models for welding.

4.1 Based on mechanical theory

Prokhorov's model assumed that when the strain accumulation exceeds a critical value, cracks may occur [103]. Prokhorov believes that the mushy area is a single entity and defines the plasticity when solidification occurs. During solidification, the ductility

of the pasty area decreases. The temperature range in which ductility decreases is called the brittle temperature range (BTR). BTR usually falls within the solidification temperature range, but due to the solute segregation and local solidus temperature drop formed by the formation of liquid film at the grain boundary, BTR can be extended to the temperature below the solidus. Strain begins to accumulate at the beginning of solidification. If a solidification crack occurs, the total cumulative strain (line A) exceeds the ductility limit (ϵ_{min}), that is, line A is steeper than the critical strain tangent. If the cumulative strain remains below ϵ_{min} , no cracks will occur. The disadvantage of this theory is that it did not consider the strain localization at the liquid film. Based on the assumption in the BTR, the difference between the sum of D_{min} and the linear free shrinkage $\Delta\epsilon_{free}$, the obvious strain $\Delta\epsilon_{app}$. And in this interval, $\Delta\epsilon_{res}$ is the minimum value, written as:

$$\Delta\epsilon_{res} = \min(D_{min} - \Delta\epsilon_{free} - \Delta\epsilon_{app}) \quad (1)$$

or

$$\frac{\Delta\epsilon_{res}}{BTR} = \frac{D_{min} - (\Delta\epsilon_{free} + \Delta\epsilon_{app})}{BTR} \quad (2)$$

Compared with Prokhorov, Novikov's thermal cracking criterion ignores apparent strain. From a mechanical point of view, the thermal crack sensitivity of alloy solidification is studied. The thermal crack is determined by the shrinkage strain in the paste relative to the fracture strain of the paste [104]. According to Novikov, during the solidification process, the alloy shrinks due to solidification shrinkage in the mushy area and thermal shrinkage nearby [105]. First, the density difference between solid metal and liquid metal causes volume shrinkage. On the other hand, the thermal

expansion coefficient of the material will affect the thermal shrinkage rate. As with welding and casting, there are constraints on the solidification process of the workpiece, such as: the rigid mold of the metal will hinder the shrinkage; the clamping of the weldment makes it difficult to release the stress during the solidification process [105]. He proposed the "plastic reserve" P_r in the solidification range, that is, the integral difference between the elongation at break ε_{fr} and the linear shrinkage ε_{sh} from the solidification temperature to the temperature of the solid phase, which is the "brittle" temperature range ΔT_{br} . Then, the hot tear sensitivity is given following:

$$p_r = \frac{1}{\Delta T_{br}} \int_{T_{coh}}^{T_{sol}} (\varepsilon_{fr} - \varepsilon_{sh}) dT \quad (3)$$

Where T_{coh} is the coherence temperature and T_{sol} is the solidus temperature.

Based on the relative strain experienced during the final solidification process. Magnin et al. [106] believe that the thermal crack sensitivity (HCS) is the quotient of the circumferential plastic strain ε_{θ} at the solidus temperature and the experimentally determined fracture strain ε_{fr} close to the solidus temperature. The standard can be used to qualitatively and quantitatively predict hot tearing was proposed:

$$HSC = \frac{\varepsilon_{\theta\theta}}{\varepsilon_{fr}} \quad (4)$$

Cracks will occur when the HCS is greater than 1.

4.2 Based on nonmechanical theory

Feurer's hot tearing theory is a non-mechanical theory, which mainly focuses on the replenishment and shrinkage of liquid metals during solidification [107], the schematic diagram of model is shown in Fig.21. Thermal cracking is caused by insufficient supplementation of liquid metal, which is related to the difficulty of the

fluid passing through the mushy area while competing with solidification shrinkage. Feurer considered two aspects, SPV and SRG, respectively representing the maximum volume flow (feed term) and volume solidification shrinkage through the dendritic network. The solid phase shrinkage rate is caused by the difference between the solid phase density and the liquid phase. The shrinkage rate is given by the following formula:

$$SPV = \frac{f_l^2 \lambda_2^2 P_s}{24\pi c^3 \eta L^2} \quad (5)$$

$$P_s = P_o + P_M - P_C \quad (6)$$

$$P_M = \bar{\rho} g h \quad (7)$$

$$\bar{\rho} = \rho_l f_l + \rho_s f_s \quad (8)$$

$$P_C = \frac{4\gamma_{SL}}{\lambda_2} \quad (9)$$

Where f_l is the volume fraction of the liquid; λ_2 is the distance between the secondary dendrite arms. P_s is the effective feed pressure; L is the length of the porous network, which is determined as the distance between the coherent position and the solidus temperature; c is the curvature constant of the dendritic network; the unit η is the viscosity of the liquid phase; γ_{SL} is the solid Liquid interface energy; $\bar{\rho}$ is the average density of the paste; g is the gravity constant; h is the distance from the melt surface; ρ_l and ρ_s are the density of the liquid and solid respectively; f_l and f_s are the liquid in the dendritic network respectively And solid volume fraction; P_o , P_M and P_C are atmospheric pressure, static pressure and capillary pressure, respectively.

$$SRG = \left(\frac{\partial \ln V}{\partial t} \right) = -\frac{1}{\bar{\rho}} \frac{\partial \bar{\rho}}{\partial t} \quad (10)$$

Where V is the volume element of the solidified paste with constant mass and t is the time.

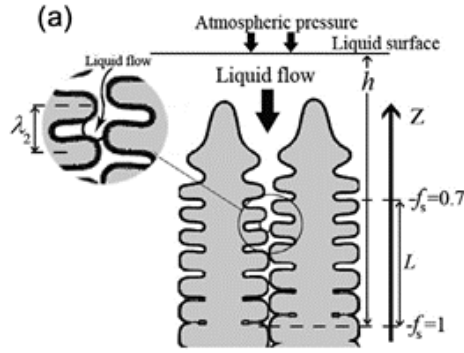


Fig.21. Schematic diagram of Feurer's hot tearing theory [107].

The hot tear criterion proposed by Clyne and Davies [108] is based on Feurer's assumption that liquid metal is difficult to move freely in the final stage of solidification, so the strain generated at this stage cannot be changed by the supplement of liquid metal. The crack sensitivity coefficient is defined by the ratio of the fragile time period t_v that may cause hot tearing to the available time t_r of the stress relief process, during which a large amount of liquid metal replenishment will occur. The hot crack sensitivity (HCS) is as follows:

$$\text{HCS} = \frac{t_v}{t_R} = \frac{t_{0.99} - t_{0.9}}{t_{0.9} - t_{0.4}} \quad (11)$$

Where $t_{0.99}$ is the time when the solid volume fraction f_s is 0.99, $t_{0.9}$ is the time when f_s is 0.9, and $t_{0.4}$ is the time when f_s is 0.4.

The model proposed by Katgerman [109] considered the casting speed, the diameter of the ingot and the alloy composition. Based on the thermal cracking theory of Clyne & Davies and Feurer, this model can be used to predict the susceptibility of hot tearing during direct cold casting of binary and commercial alloys [110]. The hot tear index is as follows:

$$\text{HCS} = \frac{t_{0.99} - t_{cr}}{t_{cr} - t_{coh}} \quad (12)$$

Among them $t_{0.99}$ is the time of $f_s=0.99$; $t_{0.4}$ is the time of $f_s=0.40$; t_{cr} is the time of insufficient feed. The time t_{cr} is determined according to Feurer's standard.

4.3 Based on both mechanical and nonmechanical theory

Rappaz, Drezet and Gremaud proposed the famous RDG model [111], which considers uniaxial tensile deformation and shrinkage feed. The supply direction of the liquid metal is opposite to the growth direction of the columnar crystals, and the direction of tensile deformation is perpendicular to the growth direction of the columnar crystals. The RDG standard is established on the basis of the late liquid feed, which is limited by the permeability of the slurry area. The closer to the front where mushy zone solidified, the higher permeability. The pressure drops along mushy area is a function of permeability and strain rate. If the local pressure is less than the critical pressure, the cavity starts. Unlike the empirical formula, this model is reasonable on the physical basis.

Braccini [112] further developed the RDG standard. Then the standards for solid-phase plastic deformation and cavity growth are proposed. The models were applied to columnar dendrites and equiaxed dendrites. Explicit relationship of critical strain rate shows that critical strain rate decreases as the solid fraction increases [112]. Wang et al. [113] considered both mechanical and metallurgical factors, and studied the effect of welding speed on solidification crack sensitivity in laser welding of 6013 aluminum alloy fiber. A finite element model of cylindrical grain size was established to calculate strain localization in the mushy area. Zhou et al. [114] used the critical diameter method to study the semi-solid hot cracking trend of 7075 alloy under different conditions. For

semi-solid slurry, increasing the mold temperature or lowering the casting temperature can significantly reduce the hot cracking trend. At the same time, the application and development of RDG guidelines were studied, solidification model shown in Fig.22 is proposed.

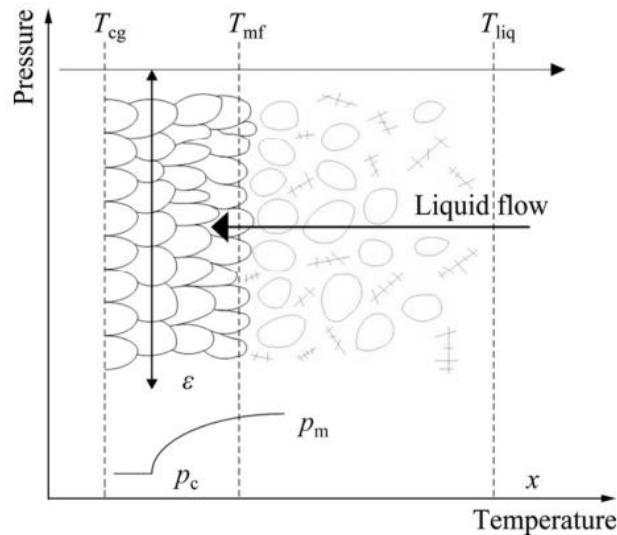


Fig.22. Schematic diagram of equiaxed dendritic growth in inoculated aluminum alloys [114].

Kou's model also targets columnar dendrites that grow in one direction. These dendrites stretch perpendicular to the growth direction and are filled with liquid metal that is opposite to the growth direction. However, unlike the RDG model, Kou's model pays more attention to the grain boundary rather than the mushy zone, including the separation of grains from each other, the lateral growth of grains to each other, and the liquid feeding between grains. The purpose of this research is not to predict whether cracks will occur during solidification, but to provide a basis for predicting the crack sensitivity of the alloy [115]. An indicator of the hot cracking of the alloy during solidification is also proposed. Different effects of $|dT/d(f_s)^{1/2}|$ near $(f_s)^{1/2} = 1$ on liquid

feeding of Al alloy A356 and Al alloy A206 are shown in Fig.23.

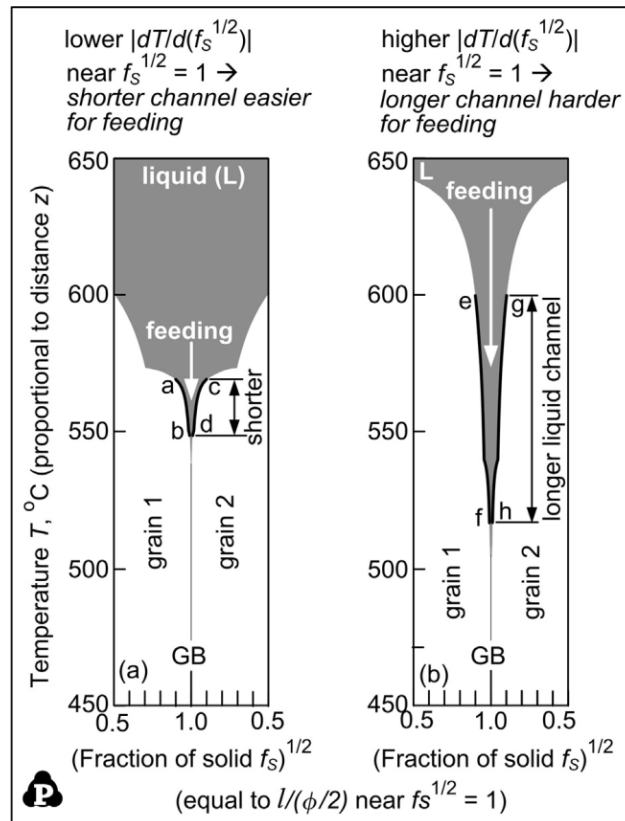


Fig.23. Effect of $|dT/d(f_s)^{1/2}|$ near $(f_s)^{1/2} = 1$ on liquid feeding: (a) Al alloy A356; (b) Al alloy A206 [115].

Fig.24 shows thin grain-boundary eutectic of Al-Sn alloys, suggesting very late extensive bridging to aggravate crack susceptibility. In order to solve some basic problems related to crack sensitivity of binary aluminum alloys in the solidification process. Liu and Kou calculated and verified the effectiveness of $|dT/d(f_s)^{1/2}|$ as a crack sensitivity index. The λ_2 of secondary dendrite arm spacing of the ordinary aluminum arc welding and the data λ_2-t_f (t_f is the local solidification time) indicate that reverse diffusion has occurred in aluminum arc welding. The binary aluminum alloy system was studied in a wide range of eutectic temperatures T_E and variable equilibrium segregation coefficient k (0-0.87). The results show that when T_E is extremely low and

the k at T_E is very high, the crack sensitivity will still be relatively low, increasing the effect of reverse diffusion on crack sensitivity reduction, which is reason for why the crack sensitivity of Al-Mg or Al-Zn is lower than that of Al-Cu. In the case of extremely low T_E and k , the crack sensitivity may be very high, which is consistent with the severe crack sensitivity of Al-Sn [116]. Still using the maximum $|dT/d(f_s)^{1/2}|$ as the crack sensitivity index, Liu and Kou calculated the crack sensitivity of the ternary aluminum alloy system. The influence of back diffusion on crack sensitivity is consistent with previous studies [117]. Han et al. [118] used Kou's standard as a function of alloying element additions to quantify the HCS of the Al-Li alloy system, the applicability of Kou's criterion in Al-Li alloy was verified.

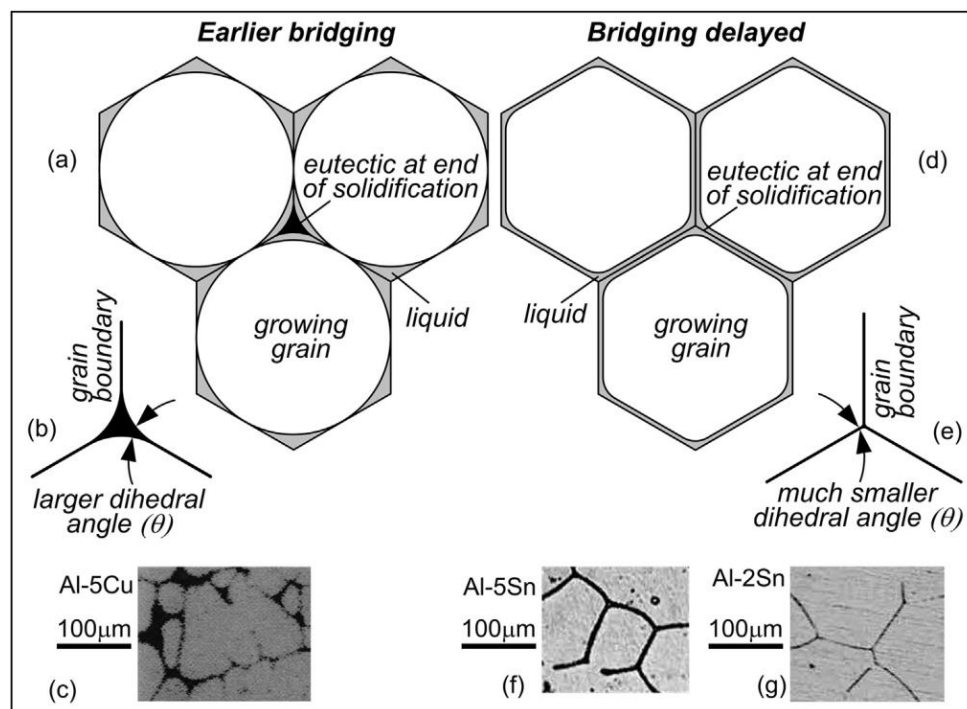


Fig.24. Thin grain-boundary eutectic of Al-Sn alloys suggesting very late extensive bridging to aggravate crack susceptibility: (a) example illustrating early initial bridging; (b) example of a relatively large angle θ ; (c) Al-5Cu [119]; (d) example

illustrating potentially very late extensive bridging; (e) example of a much smaller θ ;

(f) (g) Al-Sn alloys [119]. $f_s=0.907$ or $(f_{sB})^{1/2}=0.95$ in (a) and (d) [116].

Soysal and Kou [120] studied the effectiveness of filler metals in reducing solidification cracks in 2024 Al and 6061 Al welds. The effectiveness is evaluated by the lateral movement solderability (TMW) test, which is shown in the Fig.25. The welding results show that the filler metals 4043 Al and 4145 Al can effectively reduce the welding cracks of 2024Al, but the effect of 4145 Al is better. After the formation of the silicon-rich phase, the solid phase fraction increases rapidly during the cooling process, so that the aluminum-rich dendrites combine to resist cracking.

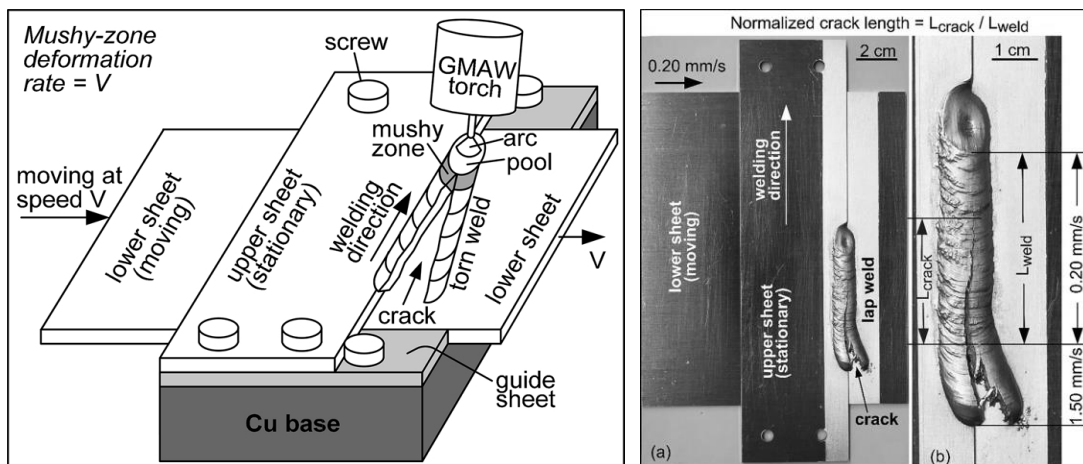


Fig.25. Schematic sketch of test used for assessing susceptibility to solidification Cracking [120].

5. Method for suppressing hot crack in pulsed laser welding

Welding residual stress significantly affects the crack growth rate of 5083 aluminum alloy [121]. In hybrid welding, cracks can be eliminated by an additional heat source. Transverse cracks shown in Fig.26 are common in laser welding and hybrid laser/arc welding of high-strength aluminum alloys. The transverse tensile strain is

mainly caused in the welding fusion zone by the cooling stage. An additional heat source can be used to change the temperature distribution, thereby reducing the tendency to crack [122]. The mechanism of hot crack is still a problem worthy of further study. Combined with the proposed criterion of hot crack sensitivity and the main research on crack solving, the mechanism of eliminating hot crack in pulsed laser welding can be considered from the following three aspects.

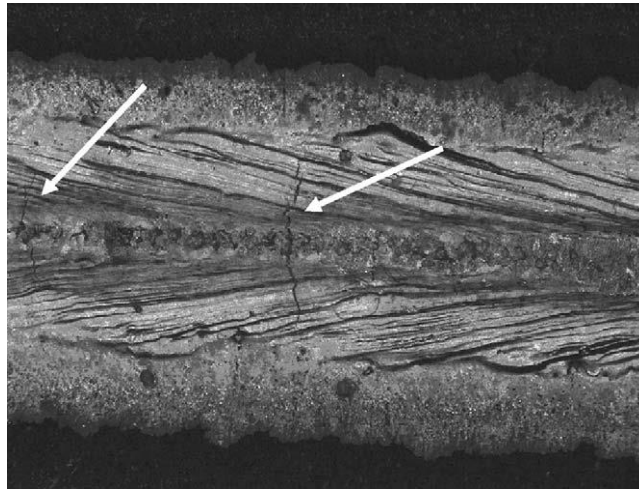


Fig.26. Typical transverse cracks found in AA7075 weld samples [122].

5.1. Phase composition and element diffusion

Generally, in alloy casting or welding, the chemical composition will have a significant impact on the hot cracking sensitivity [118]. The alloying elements will evaporate, diffuse and back diffuse during welding. Vaporization of alloy in laser welding results in changes in concentration of volatile elements Mg and Zn. Then solidification range of the welding and hot crack sensitivity changed. At a fixed average laser power, the Mg concentration of the weld metal will decrease with pulse frequency increasing, thereby reducing the interaction of Mg with other elements [123]. The simulation results of the laser spot welding process of the AA6063-T6

aluminum alloy given by Liu et al. [124] show that when the temperature is lower than the coherent temperature, the cumulative strain increases with the increase of solid fraction in the paste region. As shown in Fig.27, with the solidification process going on, the crack sensitivity near the top and middle of the weld is very high.

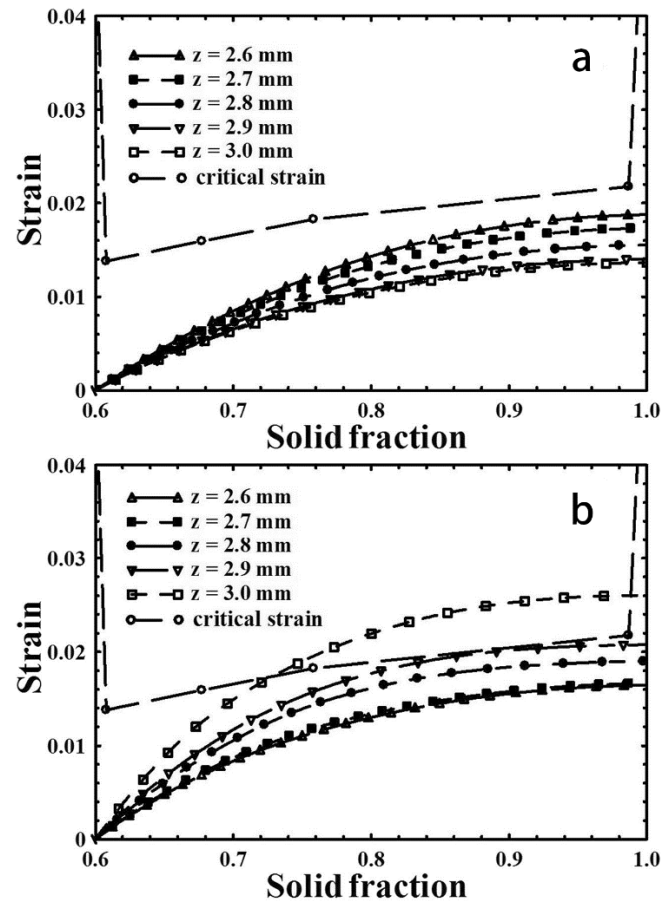


Fig.27. Effect of solute segregation on the mechanical strain in the mushy zone at $r=0.2$ mm: a) without segregation, b) with segregation [124].

Although Al-Mg alloy has a wide solidification interval, it still has good crack resistance during solidification. Liu et al. [125] found that a large amount of Mg back-diffusion occurred during the solidification process by quenching the mushy area in the arc welding process of the 5086 aluminum alloy, which made the dendritic grains combine widely to resist the earlier intergranular cracks. Effect of back diffusion on

crack susceptibility is shown in the Fig.28.

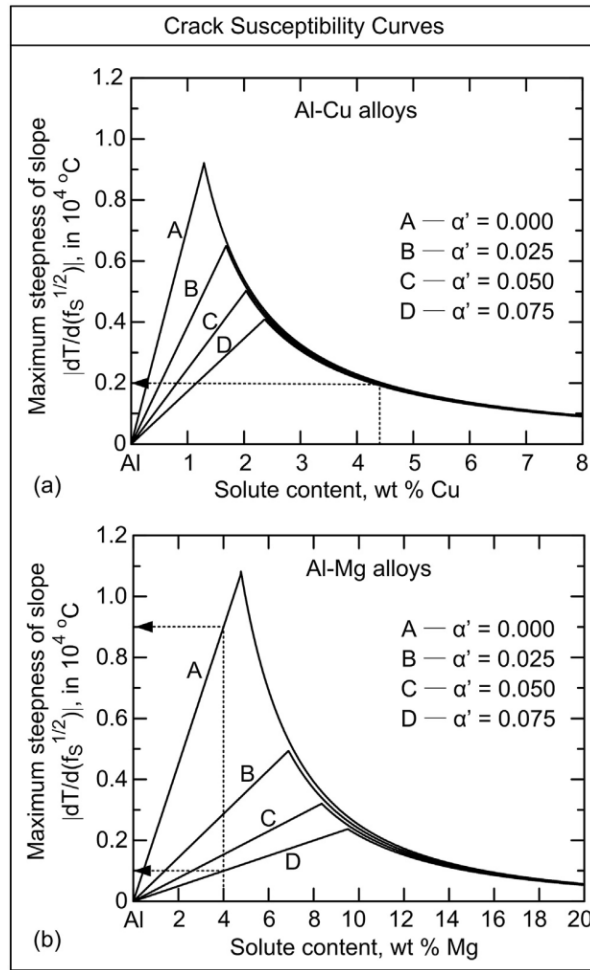


Fig.28. Effect of back diffusion on crack susceptibility: (a) Al-Cu alloys; (b) Al-Mg alloys [125].

The use of pulse shaping can improve the structure of laser welded joints, and reduce the degree of materials mixing in the molten pool, thereby improving the strength of CP-Ti and stainless steel plate dissimilar weld joints [95]. Fang et al. [98] used lower pulsed laser power to form (Cu, Nb) solid solution instead of (Nb, Ti) solid solution in the weld, successfully suppressing the formation of cracks. The calculations on Al-Mg alloy of Beiranvand et al. [60] show that the solidification rate decreases with the increase of laser pulse frequency, so the sensitivity of solidification crack is reduced.

At the same time, the Mg concentration of the final weld metal decreases due to continuous evaporation, thus increasing HCS. However, the effect of decreasing solidification rate on HCS is more obvious than that of Mg content.

5.2. Microstructure evolution

In the final stage of solidification, Agarwal et al. [126] observed liquid feeding in the inter-cellular regions, which is shown in Fig.29. The average liquid flow rate was found to be 450–500 $\mu\text{m/s}$. A pressure difference of about 104 Pa was calculated to cause the liquid to flow. It was found that the solidification shrinkage rate and deformation rate were less than the liquid feed rate.

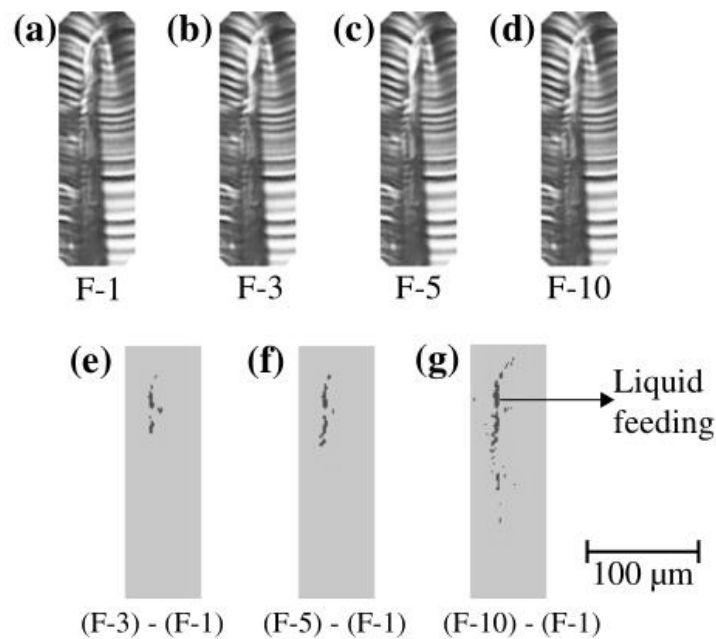


Fig.29. Solidification images: (a) Liquid flow observed in the inter-cellular and taken as the reference image, (b) liquid flow was observed, (c) and (d) liquid flow continues and reaches the bottom of the image when compared to the reference image, (e), (f) and (g) show the extent of the liquid flow in images (b), (c) and (d) when compared to reference image (a). (Using a MATLAB code to detect motion in a series of otherwise

still images) [126].

When the fusion process is used for laser welding, the 2024 aluminum alloy is prone to occur solidification cracks in the weld and liquefaction cracks in the base material. Liquefaction cracks were usually the starting point for solidification cracks. Repairing the liquefaction grain boundaries by backfilling can suppress the generation of cracks in the fusion zone. Under low laser pulse energy, the trend of crack formation reduced due to the effects of lower thermal gradients and stress [53]. Sheikhi et al. [54] proposed that for suppressing solidification cracking, the allowable solidification rate is inversely proportional to the length of the vulnerable area. And by properly controlling the ramp-down pulse shaping, solidification cracks can be avoided. The model proposed in this study can also be a good predictor of the effect of base metal initial temperature on crack sensitivity by modifying Feurer's criterion, as shown in Fig.30.

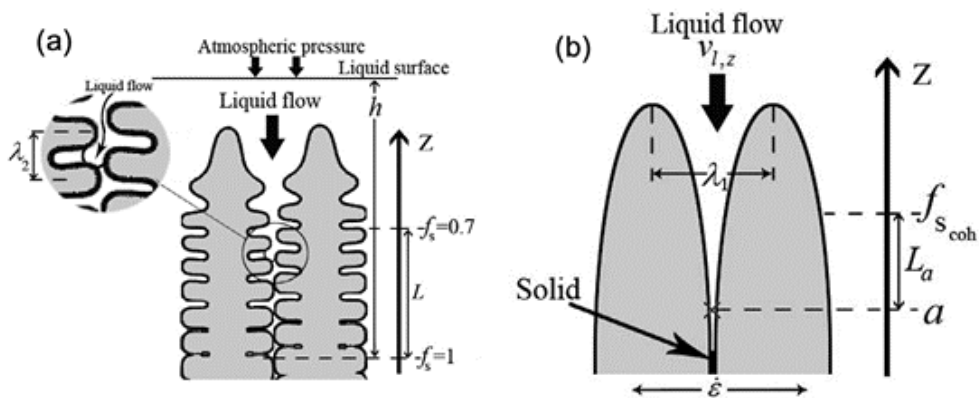


Fig.30. Schematic diagram of SPV liquid flow and influencing factors: (a) Feurer's criterion for dendritic structure; (b) modified Feurer's criterion for cellular structure.

[54].

Hekmatjou and Naffakh-Moosavy [59] found that hot cracking of the 5456

aluminum alloy pulsed laser welding can be avoided by preheating. Increasing the average laser power, pulse frequency and decreasing the pulse duration alone will also reduce the hot crack sensitivity, which is shown in the Fig.31. Mainly due to the decrease in cooling rate, which leads to the transformation of the solidification mode from columnar grains to equiaxed grains, and the backfilling of liquefied grain boundaries.

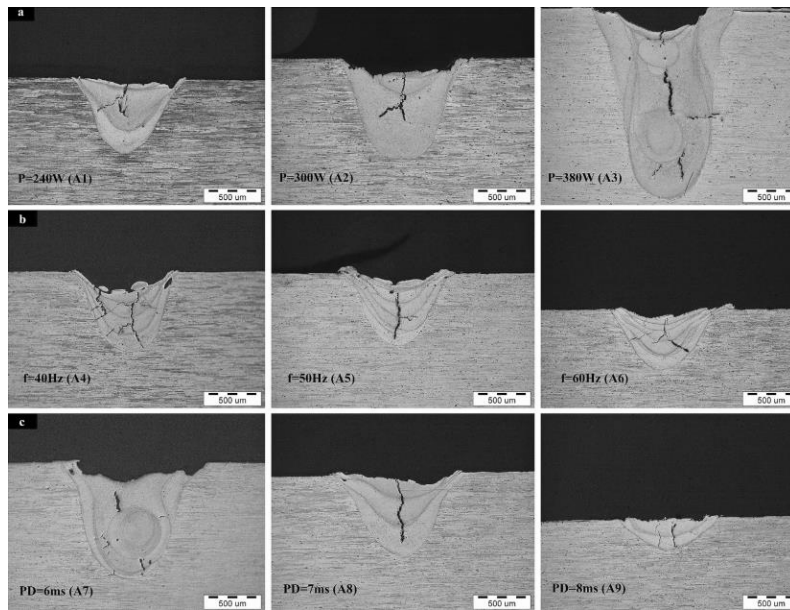


Fig.31. Change in the weld profile of aluminum alloy 5456 with pulsed laser: (a) Average power; (b) Pulse frequency; (c) Pulse duration [59].

As shown in the Fig.32, the initial crack formation direction is related to the change of solidification conditions in magnesium alloy pulsed laser welding. Under different welding conditions, initial cracks will be formed in different directions in the mushy area, and then cracks will propagate along grain boundaries. Using the pulse shaping can significantly reduce solidification rate of the molten pool, preventing initial crack formation with an aspect ratio of less than 0.8 in the sensitive direction, thereby eliminating solidification cracks [29].

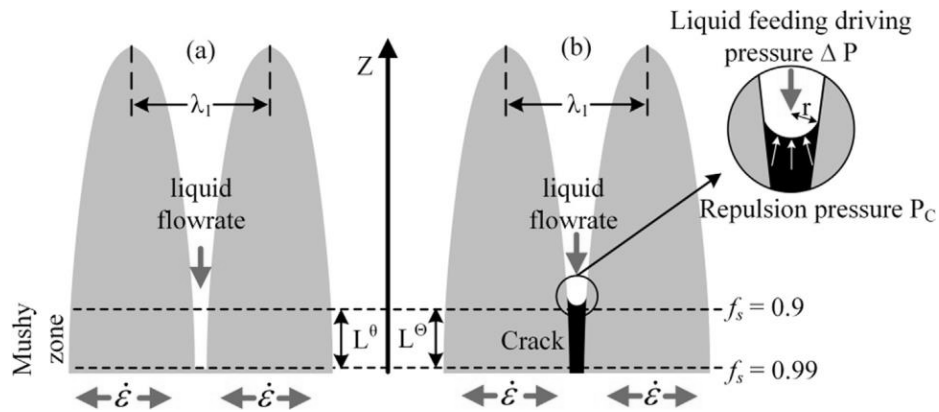


Fig.32. Schematic illustration of the strain rate and the liquid flowrate: (a) before the initial crack formation (b) after the initial crack formation [29].

It is a difficult problem to avoid liquefaction cracks of superalloy during welding. Montazeri and Ghaini [71] used pre-weld heat treatment to study the liquefaction cracking behavior of low-power pulsed Nd:YAG laser welding IN738LC. The results show that the liquefaction cracks in the alloy are mainly related to γ - γ' eutectic, MC carbide, Cr-Mo boride and Ni-Zr intermetallic compounds. During the heating cycle of welding, the boride particles reduced the onset temperature of non-equilibrium intercrystalline liquefaction in the heat affected zone. Under the rapid solidification conditions of pulsed laser welding, the current predictions of austenitic stainless-steel microstructure and welding solidification crack sensitivity were not accurate. Lippold [127] found that solidification cracks are related to the transformation of solidification behavior. When the structure is mainly austenite, it has higher crack sensitivity. Ardakani and Naffakh-Moosavy [99] eliminated dissimilar welding cracks between Kovar alloy and AISI3041 by heat input levels below 15 J/mm. Mainly due to the molten pool does not have enough time to mix, the existence of fine dendrite structure and hardening elements.

5.3. Stress development

The hot crack could be prevented by compressive load produced by thermal expansion near the weld, which balances the solidification shrinkage in the weld. During laser beam welding of AA6014 aluminum alloy, Hagenlocher et al. [128] revealed the characteristics of strain time evolution related to the formation of midline cracks in laser beam welding as shown in the Fig.33. During the initiation of hot cracks, the compressive strain first decreases, and then the tensile strain increases during the central crack propagation. When there is neither tensile strain nor significant compressive strain and strain rate during solidification, hot cracks will occur.

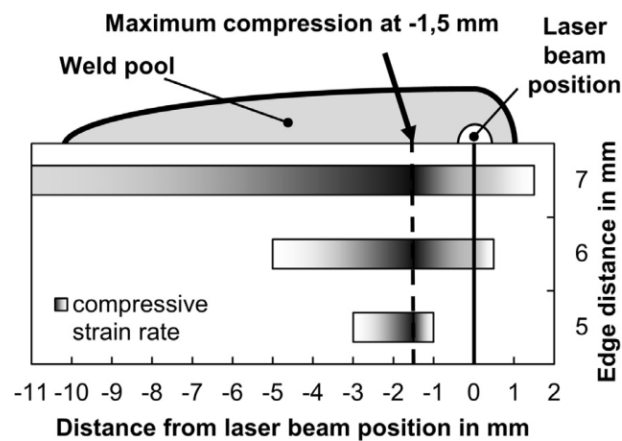


Fig.33. Influence of relative position of molten pool on negative strain rate of weld (Grayscale represents the distribution of negative strain rate) [128].

Bergmann et al. [6] improved the weldability of aluminum pulsed laser welding by superposition of a diode laser. Due to the preheating of diode laser, the absorption of welding energy is enhanced, the favorable solidification conditions are promoted, and the hot cracks are effectively avoided, which is shown in Fig.34.

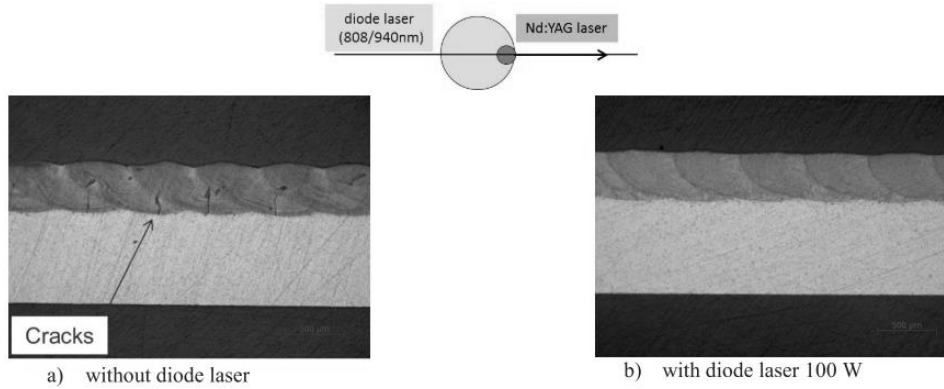


Fig.34. Influence of superposition in longitudinal cross section [6].

von Witzendorff et al. [65] found that the strain rate increases in a logarithmic manner with respect to the slope of the laser pulse's cooling time, at the condition of the interface velocity considered as an indicator for the strain rate. Then they used pulse shaping to make the rapid solidification process occur at initial stage of solidification, when molten pool had a large liquid fraction [129], the pulse shaping is shown in Fig.35, Although the experiment did not completely eliminate the solidification crack of the 6082 aluminum alloy, by reducing the crack radius and the appropriate overlap ratio between the pulses, the latter pulsed laser completely covered the cracked region of the previous pulsed laser, and finally avoided the inheritance of cracks.

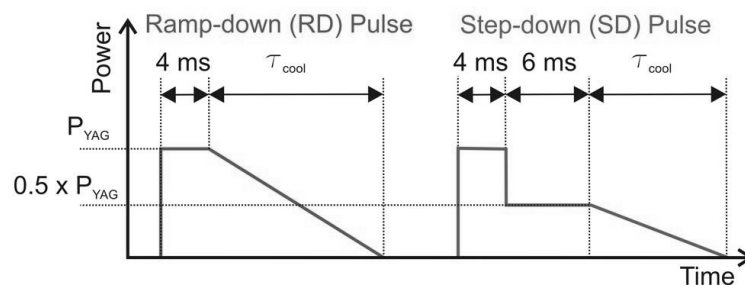


Fig.35. Pulse shaping to control temporal strain development and solidification cracking [129].

4. Summary and outlook

Compared arc welding and continuous laser welding method, applications of pulsed laser welding have a relatively short history. In the continuous welding process, additional materials are a common method to avoid defects such as cracks. However, for some micro-connection techniques involving pulsed laser welding, methods such as adding welding wire are not feasible. On the one hand, the welding preheating and cooling rates can be achieved simultaneously by editing the pulse shaping. On the other hand, adding an additional heat source is also an effective way to solve problems such as avoiding thermal cracking. In industrial applications, light metals such as aluminum alloys and magnesium alloys can not only meet the strength requirements of mechanical components, but also meet the lightweight requirements of green development products. Many problems have been proposed such as porosity and hot crack when welding aluminum alloys and magnesium alloys. It has been proved that in pulsed laser welding, the pulse shaping can be used to reduce the cooling rate in the process of welding solidification to eliminate cracks; the porosity can also be eliminated by pool oscillation or welding spot remelting. The liquefaction cracks of nickel-based superalloys are closely related to the phase composition of the base material and are also inevitable in pulsed lasers. Under the condition of low heat input of pulsed laser, it can significantly improve the welding deformation of aluminum alloy, nickel-based superalloy and stainless-steel sheet. By discussing the indexes proposed to predict the crack sensitivity of the alloy, we can more comprehensively understand the formation process and causes of the solidification crack of the alloy during the welding. Then, based on casting condition, these indexes are not applicable for the solidification conditions of rapid

cooling in the pulsed laser. Therefore, it is necessary to further optimize the crack sensitivity indexes that had been proposed and expect to be able to accurately predict the crack sensitivity of the alloy under pulsed laser welding conditions in the future.

Acknowledgements

This research was supported by National Natural Science Foundation of China (52075317, 51905333, 51805316), the Royal Society through International Exchanges 2018 Cost Share (China) scheme (IEC\NSFC\181278), Shanghai Sailing Program (19YF1418100), Shanghai Science and Technology Committee Innovation Grant (19511106400, 19511106402), Karamay Science and Technology Major Project (2018ZD002B), Shanghai Local Colleges and Universities Capacity Building Special Plan Project (19030501300).

References

- [1] A.C. Akué Asséko, B. Cosson, F. Schmidt, Y. Le Maoult, R. Gilblas, E. Lafranche, Laser transmission welding of composites - Part B: Experimental validation of numerical model, *Infrared Phys. Technol.* 73 (2015) 304–311. <https://doi.org/10.1016/j.infrared.2015.10.005>.
- [2] D. Jiang, A.S. Alsagri, M. Akbari, M. Afrand, A.A. Alrobaian, Numerical and experimental studies on the effect of varied beam diameter, average power and pulse energy in Nd: YAG laser welding of Ti6Al4V, *Infrared Phys. Technol.* 101 (2019) 180–188. <https://doi.org/10.1016/j.infrared.2019.06.006>.
- [3] A. Tur, F. Cordovilla, Á. García-Beltrán, J.L. Ocaña, Minimization of the thermal material effects on pulsed dynamic laser welding, *J. Mater. Process. Technol.* 246 (2017) 13–21. <https://doi.org/10.1016/j.jmatprotec.2017.03.007>.
- [4] G.G. Gladush, I. Smurov, Interaction of repetitively pulsed laser radiation with materials, in: *Springer Ser. Mater. Sci.*, Springer, 2011: pp. 471–527. https://doi.org/10.1007/978-3-642-19831-1_9.
- [5] F. Malek Ghaini, M.J. Hamed, M.J. Torkamany, J. Sabbaghzadeh, Weld metal microstructural characteristics in pulsed Nd: YAG laser welding, *Scr. Mater.* 56 (2007) 955–958. <https://doi.org/10.1016/j.scriptamat.2007.02.019>.
- [6] J.P. Bergmann, M. Bielenin, M. Stambke, T. Feustel, P. V. Witzendorff, J. Hermsdorf, Effects of diode laser superposition on pulsed laser welding of aluminum, *Phys. Procedia.* 41 (2013) 180–189. <https://doi.org/10.1016/j.phpro.2013.03.068>.

- [7] F. Li, W. Tao, G. Peng, J. Qu, L. Li, Behavior and stability of droplet transfer under laser-MIG hybrid welding with synchronized pulse modulations, *J. Manuf. Process.* 54 (2020) 70–79.
<https://doi.org/10.1016/j.jmapro.2020.02.017>.
- [8] J. Ning, L.J. Zhang, S.J. Na, X.Q. Yin, J. Niu, J.X. Zhang, H.R. Wang, Numerical study of the effect of laser-arc distance on laser energy coupling in pulsed Nd: YAG laser/TIG hybrid welding, *Int. J. Adv. Manuf. Technol.* 91 (2017) 1129–1143. <https://doi.org/10.1007/s00170-016-9812-9>.
- [9] Y.Z. Jia, J. Xiao, S.J. Chen, W.H. Huang, Pulsed laser enhanced metal transfer of aluminum alloy in GMAW, *Opt. Lasers Eng.* 121 (2019) 29–36.
<https://doi.org/10.1016/j.optlaseng.2019.03.011>.
- [10] O.O. Oladimeji, E. Taban, Trend and innovations in laser beam welding of wrought aluminum alloys, *Weld. World.* 60 (2016) 415–457.
<https://doi.org/10.1007/s40194-016-0317-9>.
- [11] S. Yan, Y. Shi, Influence of laser power on microstructure and mechanical property of laser-welded Al/Cu dissimilar lap joints, *J. Manuf. Process.* 45 (2019) 312–321. <https://doi.org/10.1016/j.jmapro.2019.07.009>.
- [12] A.T. Kermanidis, P.I. Christodoulou, E. Hontzopoulos, G.N. Haidemenopoulos, H. Kamoutsi, A.D. Zervaki, Mechanical performance of laser spot-welded joints in Al-Al/Cu solar thermal absorbers, *Mater. Des.* 155 (2018) 148–160. <https://doi.org/10.1016/j.matdes.2018.05.052>.
- [13] K. Mathivanan, P. Plapper, Laser welding of dissimilar copper and aluminum

- sheets by shaping the laser pulses, *Procedia Manuf.* 36 (2019) 154–162.
<https://doi.org/10.1016/j.promfg.2019.08.021>.
- [14] F. Lerra, A. Ascari, A. Fortunato, The influence of laser pulse shape and separation distance on dissimilar welding of Al and Cu films, *J. Manuf. Process.* 45 (2019) 331–339. <https://doi.org/10.1016/j.jmapro.2019.07.015>.
- [15] L. Huang, X. Hua, D. Wu, L. Fang, Experimental Investigation and Numerical Study on the Elimination of Porosity in Aluminum Alloy Laser Welding and Laser–GMA Welding, *J. Mater. Eng. Perform.* 28 (2019) 1618–1627.
<https://doi.org/10.1007/s11665-019-03955-x>.
- [16] F. Matsuda, K. Nakata, K. Tsukamoto, S. Johgan, Effect of Electromagnetic Stirring on Improvement of Solidification Crack Susceptibility of Zirconium Containing Al-Zn-Mg Alloy Weld —Fundamental Research on Solidification Crack Susceptibility of Al-Zn-Mg Alloy Weld (Report 2)—, *Q. J. Japan Weld. Soc.* 4 (1986) 120–125. <https://doi.org/10.2207/qjjws.4.120>.
- [17] H.T. Kim, S.W. Nam, Solidification cracking susceptibility of high strength aluminum alloy weldment, *Scr. Mater.* 34 (1996) 1139–1145.
[https://doi.org/10.1016/1359-6462\(95\)00644-3](https://doi.org/10.1016/1359-6462(95)00644-3).
- [18] M. Holzer, K. Hofmann, V. Mann, F. Hugger, S. Roth, M. Schmidt, Change of hot cracking susceptibility in welding of high strength aluminum alloy AA 7075, *Phys. Procedia.* 83 (2016) 463–471.
<https://doi.org/10.1016/j.phpro.2016.08.048>.
- [19] S. Petronic, S. Drecun-Nesic, A. Milosavljevic, A. Sedmak, M. Popovic, A.

- Kovacevic, Microstructure changes of nickel-base superalloys induced by Interaction with femtosecond laser beam, *Acta Phys. Pol. A.* 116 (2009) 550–552. <https://doi.org/10.12693/APhysPolA.116.550>.
- [20] O.A. Ojo, N.L. Richards, M.C. Chaturvedi, Microstructural study of weld fusion zone of TIG welded IN 738LC nickel-based superalloy, *Scr. Mater.* 51 (2004) 683–688. <https://doi.org/10.1016/j.scriptamat.2004.06.013>.
- [21] Y. Danis, C. Arvieu, E. Lacoste, T. Larrouy, J.M. Quenisset, An investigation on thermal, metallurgical and mechanical states in weld cracking of Inconel 738LC superalloy, *Mater. Des.* 31 (2010) 402–416. <https://doi.org/10.1016/j.matdes.2009.05.041>.
- [22] F. Caiazzo, V. Alfieri, F. Cardaropoli, V. Sergi, Investigation on edge joints of Inconel 625 sheets processed with laser welding, *Opt. Laser Technol.* 93 (2017) 180–186. <https://doi.org/10.1016/j.optlastec.2017.03.011>.
- [23] O.A. Ojo, N.L. Richards, M.C. Chaturvedi, Contribution of constitutional liquation of gamma prime precipitate to weld HAZ cracking of cast Inconel 738 superalloy, *Scr. Mater.* 50 (2004) 641–646. <https://doi.org/10.1016/j.scriptamat.2003.11.025>.
- [24] M. Pakniat, F.M. Ghaini, M.J. Torkamany, Hot cracking in laser welding of Hastelloy X with pulsed Nd: YAG and continuous wave fiber lasers, *Mater. Des.* 106 (2016) 177–183. <https://doi.org/10.1016/j.matdes.2016.05.124>.
- [25] T. Azimzadegan, S.A.A. Akbari Mousavi, Investigation of the occurrence of hot cracking in pulsed Nd-YAG laser welding of Hastelloy-X by numerical and

- microstructure studies, *J. Manuf. Process.* 44 (2019) 226–240.
<https://doi.org/10.1016/j.jmapro.2019.06.005>.
- [26] G. Zhang, C. Xiao, M. Taheri, Effect of Nd:YAG pulsed laser welding process on the liquation and strain-age cracking in GTD-111 superalloy, *J. Manuf. Process.* 52 (2020) 66–78. <https://doi.org/10.1016/j.jmapro.2020.01.049>.
- [27] M. Gao, H. Wang, K. Hao, H. Mu, X. Zeng, Evolutions in microstructure and mechanical properties of laser lap welded AZ31 magnesium alloy via beam oscillation, *J. Manuf. Process.* 45 (2019) 92–99.
<https://doi.org/10.1016/j.jmapro.2019.07.001>.
- [28] M. Chen, J. Xu, L. Xin, Z. Zhao, F. Wu, S. Ma, Y. Zhang, Effect of keyhole characteristics on porosity formation during pulsed laser-GTA hybrid welding of AZ31B magnesium alloy, *Opt. Lasers Eng.* 93 (2017) 139–145.
<https://doi.org/10.1016/j.optlaseng.2017.01.018>.
- [29] X. Zhang, Z. Cao, P. Zhao, Investigation on solidification cracks in pulsed laser spot welding of an AZ31 magnesium alloy, *Opt. Laser Technol.* 126 (2020) 106132. <https://doi.org/10.1016/j.optlastec.2020.106132>.
- [30] X. Zhang, Z. Cao, Effects of pulse shaping on Nd:YAG laser spot welds in an AZ31 magnesium alloy, *Opt. Lasers Eng.* 119 (2019) 1–8.
<https://doi.org/10.1016/j.optlaseng.2019.02.002>.
- [31] K. Chongbunwatana, Simulation of vapour keyhole and weld pool dynamics during laser beam welding, *Prod. Eng.* 8 (2014) 499–511.
<https://doi.org/10.1007/s11740-014-0555-x>.

- [32] Y. Luo, L. Zhu, J. Han, J. Xu, C. Zhang, D. Chen, Effect of focusing condition on laser energy absorption characteristics in pulsed laser welding, *Opt. Laser Technol.* 117 (2019) 52–63. <https://doi.org/10.1016/j.optlastec.2019.04.001>.
- [33] J. Bliedtner, H. Müller, A. Barz, *Lasermaterialbearbeitung: Grundlagen-Verfahren-Anwendungen-Beispiele*, Carl Hanser Verlag GmbH Co KG, 2013.
- [34] R. Liang, Y. Luo, Study on weld pool behaviors and ripple formation in dissimilar welding under pulsed laser, *Opt. Laser Technol.* 93 (2017) 1–8. <https://doi.org/10.1016/j.optlastec.2017.01.029>.
- [35] C. Bertrand, A. Poulon-Quintin, Temporal pulse shaping: a key parameter for the laser welding of dental alloys, *Lasers Med. Sci.* 30 (2015) 1457–1464. <https://doi.org/10.1007/s10103-014-1606-4>.
- [36] C. Zhou, H. Li, G. Chen, G. Wang, Z. Shan, Effect of single pulsed picosecond and 100 nanosecond laser cleaning on surface morphology and welding quality of aluminium alloy, *Opt. Laser Technol.* 127 (2020) 106197. <https://doi.org/10.1016/j.optlastec.2020.106197>.
- [37] A.W. Alshaer, L. Li, A. Mistry, The effects of short pulse laser surface cleaning on porosity formation and reduction in laser welding of aluminium alloy for automotive component manufacture, *Opt. Laser Technol.* 64 (2014) 162–171. <https://doi.org/10.1016/j.optlastec.2014.05.010>.
- [38] D. Banat, S. Ganguly, S. Meco, P. Harrison, Application of high power pulsed nanosecond fibre lasers in processing ultra-thin aluminium foils, *Opt. Lasers Eng.* 129 (2020). <https://doi.org/10.1016/j.optlaseng.2020.106075>.

- [39] S. Li, G. Chen, M. Zhang, Y. Zhou, Y. Zhang, Dynamic keyhole profile during high-power deep-penetration laser welding, *J. Mater. Process. Technol.* 214 (2014) 565–570. <https://doi.org/10.1016/j.jmatprotec.2013.10.019>.
- [40] D. Zhang, M. Wang, C. Shu, Y. Zhang, D. Wu, Y. Ye, Dynamic keyhole behavior and keyhole instability in high power fiber laser welding of stainless steel, *Opt. Laser Technol.* 114 (2019) 1–9. <https://doi.org/10.1016/j.optlastec.2019.01.018>.
- [41] P.G. Sanders, K.H. Leong, J.S. Keske, G. Kornecki, Real-time monitoring of laser beam welding using infrared weld emissions, *J. Laser Appl.* 10 (1998) 205–211. <https://doi.org/10.2351/1.521853>.
- [42] X. Gao, D. You, S. Katayama, Infrared image recognition for seam tracking monitoring during fiber laser welding, *Mechatronics.* 22 (2012) 370–380. <https://doi.org/10.1016/j.mechatronics.2011.09.005>.
- [43] S.H. Baik, M.S. Kim, S.K. Park, C.M. Chung, C.J. Kim, K.J. Kim, Process monitoring of laser welding using chromatic filtering of thermal radiation, *Meas. Sci. Technol.* 11 (2000) 1772–1777. <https://doi.org/10.1088/0957-0233/11/12/317>.
- [44] L. Li, D.J. Brookfield, W.M. Steen, Plasma charge sensor for in-process, non-contact monitoring of the laser welding process, *Meas. Sci. Technol.* 7 (1996) 615–626. <https://doi.org/10.1088/0957-0233/7/4/019>.
- [45] Y. Luo, L. Zhu, J. Han, X. Xie, R. Wan, Y. Zhu, Study on the acoustic emission effect of plasma plume in pulsed laser welding, *Mech. Syst. Signal*

- Process. 124 (2019) 715–723. <https://doi.org/10.1016/j.ymsp.2019.01.045>.
- [46] F. Lange, A. Artinov, M. Bachmann, M. Rethmeier, K. Hilgenberg, Numerical simulation of the weld pool dynamics during pulsed laser welding using adapted heat source models, *Procedia CIRP*. 74 (2018) 679–682. <https://doi.org/10.1016/j.procir.2018.08.044>.
- [47] J. Xu, Y. Rong, Y. Huang, P. Wang, C. Wang, Keyhole-induced porosity formation during laser welding, *J. Mater. Process. Technol.* 252 (2018) 720–727. <https://doi.org/10.1016/j.jmatprotec.2017.10.038>.
- [48] N. Bakir, A. Gumenyuk, M. Rethmeier, Investigation of solidification cracking susceptibility during laser beam welding using an in-situ observation technique, *Sci. Technol. Weld. Join.* 23 (2018) 234–240. <https://doi.org/10.1080/13621718.2017.1367550>.
- [49] M. Miyagi, Y. Kawahito, H. Wang, H. Kawakami, T. Shoubu, M. Tsukamoto, X-ray phase contrast observation of solidification and hot crack propagation in laser spot welding of aluminum alloy, *Opt. Express*. 26 (2018) 22626. <https://doi.org/10.1364/oe.26.022626>.
- [50] S. Geng, P. Jiang, X. Shao, G. Mi, H. Wu, Y. Ai, C. Wang, C. Han, R. Chen, W. Liu, Comparison of solidification cracking susceptibility between Al-Mg and Al-Cu alloys during welding: A phase-field study, *Scr. Mater.* 150 (2018) 120–124. <https://doi.org/10.1016/j.scriptamat.2018.03.013>.
- [51] R.K. Gupta, S.V.S.N. Murty, Analysis of crack in aluminium alloy AA2219 weldment, *Eng. Fail. Anal.* 13 (2006) 1370–1375.

- <https://doi.org/10.1016/j.engfailanal.2005.10.009>.
- [52] J. Ahn, L. Chen, E. He, J.P. Dear, C.M. Davies, Optimisation of process parameters and weld shape of high power Yb-fibre laser welded 2024-T3 aluminium alloy, *J. Manuf. Process.* 34 (2018) 70–85.
<https://doi.org/10.1016/j.jmapro.2018.05.028>.
- [53] F.M. Ghaini, M. Sheikhi, M.J. Torkamany, J. Sabbaghzadeh, The relation between liquation and solidification cracks in pulsed laser welding of 2024 aluminium alloy, *Mater. Sci. Eng. A.* 519 (2009) 167–171.
<https://doi.org/10.1016/j.msea.2009.04.056>.
- [54] M. Sheikhi, F. Malek Ghaini, H. Assadi, Prediction of solidification cracking in pulsed laser welding of 2024 aluminum alloy, *Acta Mater.* 82 (2015) 491–502.
<https://doi.org/10.1016/j.actamat.2014.09.002>.
- [55] W. Chen, P. Molian, Dual-beam laser welding of ultra-thin AA 5052-H19 aluminum, *Int. J. Adv. Manuf. Technol.* 39 (2008) 889–897.
<https://doi.org/10.1007/s00170-007-1278-3>.
- [56] M. Rohde, C. Markert, W. Pfleging, Laser micro-welding of aluminum alloys: Experimental studies and numerical modeling, *Int. J. Adv. Manuf. Technol.* 50 (2010) 207–215. <https://doi.org/10.1007/s00170-009-2510-0>.
- [57] T.E. ABIOYE, H. ZUHAILAWATI, S. AIZAD, A.S. ANASYIDA, Geometrical, microstructural and mechanical characterization of pulse laser welded thin sheet 5052-H32 aluminium alloy for aerospace applications, *Trans. Nonferrous Met. Soc. China (English Ed.)* 29 (2019) 667–679.

- [https://doi.org/10.1016/S1003-6326\(19\)64977-0](https://doi.org/10.1016/S1003-6326(19)64977-0).
- [58] S. Li, G. Mi, C. Wang, A study on laser beam oscillating welding characteristics for the 5083 aluminum alloy: Morphology, microstructure and mechanical properties, *J. Manuf. Process.* 53 (2020) 12–20.
<https://doi.org/10.1016/j.jmapro.2020.01.018>.
- [59] H. Hekmatjou, H. Naffakh-Moosavy, Hot cracking in pulsed Nd:YAG laser welding of AA5456, *Opt. Laser Technol.* 103 (2018) 22–32.
<https://doi.org/10.1016/j.optlastec.2018.01.020>.
- [60] Z.M. Beiranvand, F.M. Ghaini, H.N. Moosavy, M. Sheikhi, M.J. Torkamany, Solidification cracking susceptibility in pulsed laser welding of Al–Mg alloys, *Materialia.* 7 (2019) 100417. <https://doi.org/10.1016/j.mtla.2019.100417>.
- [61] R. Hajavifard, M. Motahari, H. Özden, H. Miyanaji, S. Kafashi, The Effects of Pulse Shaping Variation in Laser Spot-Welding of Aluminum, *Procedia Manuf.* 5 (2016) 232–247. <https://doi.org/10.1016/j.promfg.2016.08.021>.
- [62] D. Jun, L. Zheng, Y. Li, W. Yang, Z. Chiyu, Z. Yaocheng, Research on pulsed laser welding of TiB₂-enhanced aluminum matrix composites, *Int. J. Adv. Manuf. Technol.* 85 (2016) 157–162. <https://doi.org/10.1007/s00170-015-7887-3>.
- [63] Y. Kawahito, S. Katayama, In-process monitoring and adaptive control for lap welds of aluminum alloy sheets, 24th Int. Congr. Appl. Lasers Electro-Optics, ICALEO 2005 - Congr. Proc. 17 (2005) 905–914.
<https://doi.org/10.2351/1.5060480>.

- [64] M.J. Cieslak, P.W. Fuerschbach, On the weldability, composition, and hardness of pulsed and continuous Nd:YAG laser welds in aluminum alloys 6061,5456, and 5086, *Metall. Trans. B.* 19 (1988) 319–329.
<https://doi.org/10.1007/BF02654217>.
- [65] P. von Witzendorff, S. Kaierle, O. Suttman, L. Overmeyer, In Situ Observation of Solidification Conditions in Pulsed Laser Welding of AL6082 Aluminum Alloys to Evaluate Their Impact on Hot Cracking Susceptibility, *Metall. Mater. Trans. A Phys. Metall. Mater. Sci.* 46 (2015) 1678–1688.
<https://doi.org/10.1007/s11661-015-2749-z>.
- [66] B.C. Kim, T.H. Kim, J.S. Kim, K.B. Kim, H.Y. Lee, Investigation on the effect of laser pulse shape during Nd:YAG laser microwelding of thin Al sheet by numerical simulation, *Metall. Mater. Trans. A Phys. Metall. Mater. Sci.* 33 (2002) 1449–1459. <https://doi.org/10.1007/s11661-002-0068-7>.
- [67] Y. Guo, D. Wu, G. Ma, D. Guo, Trailing heat sink effects on residual stress and distortion of pulsed laser welded Hastelloy C-276 thin sheets, *J. Mater. Process. Technol.* 214 (2014) 2891–2899.
<https://doi.org/10.1016/j.jmatprotec.2014.06.012>.
- [68] G. Ma, D. Wu, F. Niu, H. Zou, Microstructure evolution and mechanical property of pulsed laser welded Ni-based superalloy, *Opt. Lasers Eng.* 72 (2015) 39–46. <https://doi.org/10.1016/j.optlaseng.2015.03.009>.
- [69] G. Shanthos Kumar, K. Raghukandan, S. Saravanan, N. Sivagurumanikandan, Optimization of parameters to attain higher tensile strength in pulsed Nd: YAG

- laser welded Hastelloy C-276–Monel 400 sheets, *Infrared Phys. Technol.* 100 (2019) 1–10. <https://doi.org/10.1016/j.infrared.2019.05.002>.
- [70] A. Bagchi, S. Saravanan, G. Shanthos Kumar, G. Murugan, K. Raghukandan, Numerical simulation and optimization in pulsed Nd: YAG laser welding of Hastelloy C-276 through Taguchi method and artificial neural network, *Optik (Stuttg.)*. 146 (2017) 80–89. <https://doi.org/10.1016/j.ijleo.2017.08.082>.
- [71] M. Montazeri, F.M. Ghaini, The liquation cracking behavior of IN738LC superalloy during low power Nd:YAG pulsed laser welding, *Mater. Charact.* 67 (2012) 65–73. <https://doi.org/10.1016/j.matchar.2012.02.019>.
- [72] G. Shanthos Kumar, S. Saravanan, R. Vetriselvan, K. Raghukandan, Numerical and experimental studies on the effect of varied pulse energy in Nd:YAG laser welding of Monel 400 sheets, *Infrared Phys. Technol.* 93 (2018) 184–191. <https://doi.org/10.1016/j.infrared.2018.08.002>.
- [73] Z. Jiang, W. Tao, K. Yu, C. Tan, Y. Chen, L. Li, Z. Li, Comparative study on fiber laser welding of GH3535 superalloy in continuous and pulsed waves, *Mater. Des.* 110 (2016) 728–739. <https://doi.org/10.1016/j.matdes.2016.08.055>.
- [74] N. Kumar, M. Mukherjee, A. Bandyopadhyay, Comparative study of pulsed Nd:YAG laser welding of AISI 304 and AISI 316 stainless steels, *Opt. Laser Technol.* 88 (2017) 24–39. <https://doi.org/10.1016/j.optlastec.2016.08.018>.
- [75] J.T. Liu, D.C. Weckman, H.W. Kerr, The effects of process variables on pulsed Nd:YAG laser spot welds: Part I. AISI 409 stainless steel, *Metall. Trans. B.* 24 (1993) 1065–1076. <https://doi.org/10.1007/BF02660998>.

- [76] W. Meng, Z. Xu, Q. Ma, X. Yin, J. Fang, Pulse fiber laser welding of AISI 321-AISI 405 stainless steel thick plates butt joints, *J. Mater. Process. Technol.* 271 (2019) 214–225. <https://doi.org/10.1016/j.jmatprotec.2019.04.013>.
- [77] A. Jayanthi, K. Venkatramanan, K. Suresh Kumar, Conductive and convective heat transfer during welding of AISI316L stainless steel using pulsed Nd: YAG laser, *Mater. Today Proc.* 22 (2020) 465–472. <https://doi.org/10.1016/j.matpr.2019.07.721>.
- [78] A. Torabi, F. Kolahan, Optimizing pulsed Nd:YAG laser beam welding process parameters to attain maximum ultimate tensile strength for thin AISI316L sheet using response surface methodology and simulated annealing algorithm, *Opt. Laser Technol.* 103 (2018) 300–310. <https://doi.org/10.1016/j.optlastec.2017.12.042>.
- [79] M. Doubenskaia, I. Smurov, Surface temperature evolution in pulsed laser action of millisecond range, *Appl. Surf. Sci.* 252 (2006) 4472–4476. <https://doi.org/10.1016/j.apsusc.2005.07.164>.
- [80] S. Saravanan, K. Raghukandan, N. Sivagurumanikandan, Pulsed Nd: YAG laser welding and subsequent post-weld heat treatment on super duplex stainless steel, *J. Manuf. Process.* 25 (2017) 284–289. <https://doi.org/10.1016/j.jmapro.2016.12.015>.
- [81] M. Bahrami Balajaddeh, H. Naffakh-Moosavy, Pulsed Nd:YAG laser welding of 17-4 PH stainless steel: Microstructure, mechanical properties, and weldability investigation, *Opt. Laser Technol.* 119 (2019).

- <https://doi.org/10.1016/j.optlastec.2019.105651>.
- [82] M.R. Pakmanesh, M. Shamanian, Optimization of pulsed laser welding process parameters in order to attain minimum underfill and undercut defects in thin 316L stainless steel foils, *Opt. Laser Technol.* 99 (2018) 30–38.
<https://doi.org/10.1016/j.optlastec.2017.09.047>.
- [83] F. Mirakhorli, F. Malek Ghaini, M.J. Torkamany, Development of weld metal microstructures in pulsed laser welding of duplex stainless steel, *J. Mater. Eng. Perform.* 21 (2012) 2173–2176. <https://doi.org/10.1007/s11665-012-0141-3>.
- [84] T. Zacharia, S.A. David, J.M. Vitek, T. Debroy, Heat transfer during Nd: Yag pulsed laser welding and its effect on solidification structure of austenitic stainless steels, *Metall. Trans. A.* 20 (1989) 957–967.
<https://doi.org/10.1007/BF02651661>.
- [85] S. Chatterjee, S.S. Mahapatra, V. Bharadwaj, B.N. Upadhyay, K.S. Bindra, J. Thomas, Parametric appraisal of mechanical and metallurgical behavior of butt welded joints using pulsed Nd:YAG laser on thin sheets of AISI 316, *Opt. Laser Technol.* 117 (2019) 186–199.
<https://doi.org/10.1016/j.optlastec.2019.04.004>.
- [86] H. Xu, X. Guo, Y. Lei, J. Lin, H. Fu, R. Xiao, T. Huang, Y.C. Shin, Welding deformation of ultra-thin 316 stainless steel plate using pulsed laser welding process, *Opt. Laser Technol.* 119 (2019) 105583.
<https://doi.org/10.1016/j.optlastec.2019.105583>.
- [87] N. Kumar, M. Mukherjee, A. Bandyopadhyay, Study on laser welding of

- austenitic stainless steel by varying incident angle of pulsed laser beam, *Opt. Laser Technol.* 94 (2017) 296–309.
<https://doi.org/10.1016/j.optlastec.2017.04.008>.
- [88] M. Chen, L. Xin, Q. Zhou, L. He, F. Wu, Effect of laser pulse on alternative current arc discharge during laser-arc hybrid welding of magnesium alloy, *Opt. Lasers Eng.* 100 (2018) 208–215.
<https://doi.org/10.1016/j.optlaseng.2017.08.017>.
- [89] P. Stritt, C. Hagenlocher, C. Kizler, R. Weber, C. Rüttimann, T. Graf, Laser spot welding of copper-aluminum joints using a pulsed dual wavelength laser at 532 and 1064 nm, *Phys. Procedia.* 56 (2014) 759–767.
<https://doi.org/10.1016/j.phpro.2014.08.083>.
- [90] M.J. Torkamany, S. Tahamtan, J. Sabbaghzadeh, Dissimilar welding of carbon steel to 5754 aluminum alloy by Nd:YAG pulsed laser, *Mater. Des.* 31 (2010) 458–465. <https://doi.org/10.1016/j.matdes.2009.05.046>.
- [91] Y. Li, Y. Liu, J. Yang, First principle calculations and mechanical properties of the intermetallic compounds in a laser welded steel/aluminum joint, *Opt. Laser Technol.* 122 (2020) 105875. <https://doi.org/10.1016/j.optlastec.2019.105875>.
- [92] R. Indhu, S. Soundarapandian, L. Vijayaraghavan, Yb: YAG laser welding of dual phase steel to aluminium alloy, *J. Mater. Process. Technol.* 262 (2018) 411–421. <https://doi.org/10.1016/j.jmatprotec.2018.05.022>.
- [93] J. Yang, Y.L. Li, H. Zhang, Microstructure and mechanical properties of pulsed laser welded Al/steel dissimilar joint, *Trans. Nonferrous Met. Soc. China*

- (English Ed. 26 (2016) 994–1002. [https://doi.org/10.1016/S1003-6326\(16\)64196-1](https://doi.org/10.1016/S1003-6326(16)64196-1).
- [94] R. Indhu, S. Divya, M. Tak, S. Soundarapandian, Microstructure development in Pulsed Laser Welding of Dual Phase Steel to Aluminium Alloy, *Procedia Manuf.* 26 (2018) 495–502. <https://doi.org/10.1016/j.promfg.2018.07.058>.
- [95] H.C. Chen, G. Bi, B.Y. Lee, C.K. Cheng, Laser welding of CP Ti to stainless steel with different temporal pulse shapes, *J. Mater. Process. Technol.* 231 (2016) 58–65. <https://doi.org/10.1016/j.jmatprotec.2015.12.016>.
- [96] S. Zhou, D. Chai, J. Yu, G. Ma, D. Wu, Microstructure characteristic and mechanical property of pulsed laser lap-welded nickel-based superalloy and stainless steel, *J. Manuf. Process.* 25 (2017) 220–226. <https://doi.org/10.1016/j.jmapro.2016.11.010>.
- [97] Y. Zhang, Y. Chen, J. Zhou, D. Sun, X. Gu, Forming mechanism and mechanical property of pulsed laser welded Ti alloy and stainless steel joint using copper as interlayer, *J. Mater. Res. Technol.* 9 (2020) 1425–1433. <https://doi.org/10.1016/j.jmrt.2019.11.068>.
- [98] Y. Fang, X. Jiang, T. Song, D. Mo, Z. Luo, Pulsed laser welding of Ti-6Al-4V titanium alloy to AISI 316L stainless steel using Cu/Nb bilayer, *Mater. Lett.* 244 (2019) 163–166. <https://doi.org/10.1016/j.matlet.2019.02.075>.
- [99] H.A. Ardakani, H. Naffakh-Moosavy, The effect of pulsed Nd:YAG laser welding parameters on defects of Kovar to AISI 304L dissimilar joint, *Opt. Laser Technol.* 118 (2019) 62–68.

- <https://doi.org/10.1016/j.optlastec.2019.05.003>.
- [100] L. Liu, J. Shi, Z. Hou, G. Song, Effect of distance between the heat sources on the molten pool stability and burn-through during the pulse laser-GTA hybrid welding process, *J. Manuf. Process.* 34 (2018) 697–705.
<https://doi.org/10.1016/j.jmapro.2018.06.038>.
- [101] I. Bunaziv, O.M. Akselsen, A. Salminen, A. Unt, Fiber laser-MIG hybrid welding of 5 mm 5083 aluminum alloy, *J. Mater. Process. Technol.* 233 (2016) 107–114. <https://doi.org/10.1016/j.jmatprotec.2016.02.018>.
- [102] J. Sun, H. Wang, L. Liu, The Analysis on the Formation of Porosity During Pulsed Laser–Induced TIG Hybrid Welding of 6061 Aluminium Alloy at High Welding Speed, *Int. J. Precis. Eng. Manuf.* 21 (2020) 1469–1477.
<https://doi.org/10.1007/s12541-019-00032-0>.
- [103] N.N. Prokhorov, Resistance to hot tearing of cast metals during solidification, *Russ. Cast. Prod.* 2 (1962) 172–75.
- [104] Suyitno, W.H. Kool, L. Katgerman, Hot tearing criteria evaluation for direct-chill casting of an Al-4.5 pct Cu alloy, *Metall. Mater. Trans. A Phys. Metall. Mater. Sci.* 36 (2005) 1537–1546. <https://doi.org/10.1007/s11661-005-0245-6>.
- [105] I. Novikov, Hot-Shortness of Nonferrous Metals and Alloys, Defense Technical Information Center, 1968.
<https://books.google.com.hk/books?id=e7p5NwAACAAJ>.
- [106] B. Magnin, L. Katgerman, B. Hannart, Physical and numerical modelling of thermal stress generation during DC casting of aluminum alloys, *Minerals*,

- Metals and Materials Society, Warrendale, PA (United States), 1995.
- [107] U. Feurer, *Quality Control of Engineering Alloys and the Role of Metals Science*, Delft Univ. Technol. Delft, Netherlands. (1977) 131–145.
- [108] T.W. Clyne, G.J. Davies, Comparison between experimental data and theoretical predictions relating to dependence of solidification cracking on composition, in: *Solidif. Cast. Met.*, 1979: p. 275.
- [109] D.L. Katgerman, D.G. Eskin, In search of the prediction of hot cracking in aluminium alloys, *Hot Crack. Phenom. Welds II*. (2008) 3–18.
https://doi.org/10.1007/978-3-540-78628-3_1.
- [110] D.G. Eskin, Suyitno, L. Katgerman, Mechanical properties in the semi-solid state and hot tearing of aluminium alloys, *Prog. Mater. Sci.* 49 (2004) 629–711.
[https://doi.org/10.1016/S0079-6425\(03\)00037-9](https://doi.org/10.1016/S0079-6425(03)00037-9).
- [111] M. Rappaz, J.-M. Drezet, M. Gremaud, A new hot-tearing criterion, *Metall. Mater. Trans. A.* 30 (1999) 449–455.
- [112] S.L. Cockcroft, D.M. Maijer, Modeling of Casting, Welding, and Advanced Solidification Processes - XII: Preface, Proc. from 12th Int. Conf. Model. Cast. Welding, *Adv. Solidif. Process.* (2009) 18–24.
- [113] X. Wang, F. Lu, H.P. Wang, Z. Qu, L. Xia, Micro-scale model based study of solidification cracking formation mechanism in Al fiber laser welds, *J. Mater. Process. Technol.* 231 (2016) 18–26.
<https://doi.org/10.1016/j.jmatprotec.2015.12.006>.
- [114] B. ZHOU, S. LU, K. le XU, C. XU, Z. yong WANG, B. jun WANG, Hot

- cracking tendency test and simulation of 7075 semi-solid aluminium alloy,
Trans. Nonferrous Met. Soc. China (English Ed. 30 (2020) 318–332.
[https://doi.org/10.1016/S1003-6326\(20\)65215-3](https://doi.org/10.1016/S1003-6326(20)65215-3).
- [115] S. Kou, A criterion for cracking during solidification, *Acta Mater.* 88 (2015) 366–374. <https://doi.org/10.1016/j.actamat.2015.01.034>.
- [116] J. Liu, S. Kou, Crack susceptibility of binary aluminum alloys during solidification, *Acta Mater.* 110 (2016) 84–94.
<https://doi.org/10.1016/j.actamat.2016.03.030>.
- [117] J. Liu, S. Kou, Susceptibility of ternary aluminum alloys to cracking during solidification, *Acta Mater.* 125 (2017) 513–523.
<https://doi.org/10.1016/j.actamat.2016.12.028>.
- [118] J. Han, J. Wang, M. Zhang, K. Niu, Susceptibility of lithium containing aluminum alloys to cracking during solidification, *Materialia.* 5 (2019) 100203.
<https://doi.org/10.1016/j.mtla.2018.100203>.
- [119] Y. Ju, L. Arnberg, Measurement of grain bridging in some Al-Cu and Al-Sn alloys, *Int. J. Cast Met. Res.* 16 (2003) 522–530.
<https://doi.org/10.1080/13640461.2003.11819630>.
- [120] T. Soysal, S. Kou, Effect of filler metals on solidification cracking susceptibility of Al alloys 2024 and 6061, *J. Mater. Process. Technol.* 266 (2019) 421–428. <https://doi.org/10.1016/j.jmatprotec.2018.11.022>.
- [121] K. Shankar, W. Wu, Effect of welding and weld repair on crack propagation behaviour in aluminium alloy 5083 plates, *Mater. Des.* 23 (2002) 201–208.

- [https://doi.org/10.1016/s0261-3069\(01\)00059-0](https://doi.org/10.1016/s0261-3069(01)00059-0).
- [122] B. Hu, I.M. Richardson, Mechanism and possible solution for transverse solidification cracking in laser welding of high strength aluminium alloys, *Mater. Sci. Eng. A.* 429 (2006) 287–294.
<https://doi.org/10.1016/j.msea.2006.05.040>.
- [123] Z.M. Beiranvand, F.M. Ghaini, H. Naffakh-moosavy, M. Sheikhi, M.J. Torkamany, Magnesium Loss in Nd:YAG Pulsed Laser Welding of Aluminum Alloys, *Metall. Mater. Trans. B Process Metall. Mater. Process. Sci.* 49 (2018) 2896–2905. <https://doi.org/10.1007/s11663-018-1315-7>.
- [124] J. Liu, Z. Rao, S. Liao, P.C. Wang, Modeling of transport phenomena and solidification cracking in laser spot bead-on-plate welding of AA6063-T6 alloy. Part II - Simulation results and experimental validation, *Int. J. Adv. Manuf. Technol.* 74 (2014) 285–296. <https://doi.org/10.1007/s00170-014-5935-z>.
- [125] J. Liu, H.P. Duarte, S. Kou, Evidence of back diffusion reducing cracking during solidification, *Acta Mater.* 122 (2017) 47–59.
<https://doi.org/10.1016/j.actamat.2016.09.037>.
- [126] G. Agarwal, M. Amirthalingam, S.C. Moon, R.J. Dippenaar, I.M. Richardson, M.J.M. Hermans, Experimental evidence of liquid feeding during solidification of a steel, *Scr. Mater.* 146 (2018) 105–109.
<https://doi.org/10.1016/j.scriptamat.2017.11.003>.
- [127] J. LIPPOLD, Solidification behavior and cracking susceptibility of pulsed-laser

- welds in austenitic stainless steels, *Weld. J.* 73 (1994) 129.
- [128] C. Hagenlocher, P. Stritt, R. Weber, T. Graf, Strain signatures associated to the formation of hot cracks during laser beam welding of aluminum alloys, *Opt. Lasers Eng.* 100 (2018) 131–140.
<https://doi.org/10.1016/j.optlaseng.2017.08.007>.
- [129] P. Von Witzendorff, S. Kaierle, O. Suttman, L. Overmeyer, Using pulse shaping to control temporal strain development and solidification cracking in pulsed laser welding of 6082 aluminum alloys, *J. Mater. Process. Technol.* 225 (2015) 162–169. <https://doi.org/10.1016/j.jmatprotec.2015.06.007>.

Declaration of interests

The authors declare that they have no known competing financial interests or personal relationships that could have appeared to influence the work reported in this paper.

The authors declare the following financial interests/personal relationships which may be considered as potential competing interests: